# Uniqueness conditions in a hyperbolic model for oil recovery by steamdrive

J. Bruining [a] and C.J. van Duijn [b,c]

[a] *Dietz Laboratory, Centre of Technical Geoscience, Mijnbouwstraat 120, 2628 RX Delft, The Netherlands*
E-mail: j.bruining@ta.tudelft.nl
[b] *Centre for Mathematics and Computer Science (CWI), P.O. Box 94079, 1090 GB Amsterdam, The Netherlands*
[c] *Department of Applied Mathematics, Delft University of Technology, Delft, The Netherlands*
E-mail: hansd@cwi.nl

Received 11 February 2000

In this paper we study a one-dimensional model for oil recovery by steamdrive. This model consists of two parts: a (global) interface model and a (local) steam condensation/capillary diffusion model. In the interface model a steam condensation front (SCF) is present as an internal boundary between the hot steam zone (containing water, oil and steam) and the cold liquid zone (containing only water and oil). Disregarding capillary pressure away from the SCF, a $2 \times 2$ hyperbolic system arises for the water and steam saturation. This system cannot be solved uniquely without additional conditions at the SCF. To find such conditions we blow up the SCF and consider a parabolic transition model, including capillary diffusion. We study in detail the existence conditions for traveling wave solutions. These conditions provide the missing matching conditions at the SCF in the hyperbolic limit. We show that different transition models yield different matching conditions, and thus different solutions of the interface model. We also give a relatively straightforward approximation and investigate its validity for certain ranges of model parameters.

**Keywords:** multi-phase flow, porous media, hyperbolic system, (non-)uniqueness, traveling waves

## 1. Introduction

Steamdrive, being the most important enhanced oil recovery technique, received considerable attention in the engineering literature during the past decades. As examples we mention the experimental work of Kimber et al. [17], Gümrah et al. [11] and Farouq Ali et al. [7], and the modeling work of Mandl and Volek [20], Godderij et al. [10] and Prats [25]. An important characteristic of their models is the occurrence of a Steam Condensation Front (SCF) as an internal boundary between the hot steam zone and the cold liquid zone. Furthermore, in their approach the saturation of the oil

remaining behind in the steam zone does not follow from the analysis of the models, but is a priori given as a model parameter.

Shutler [27] proposed a relatively simple model which treats the oil saturation in the steam zone as unknown. We explain it here in some detail because it forms the basis for our approach. In this model again a SCF is present, which separates an upstream steam zone from a downstream oil/water zone. It is assumed that all steam condenses at the SCF. The velocity of the SCF follows from a local heat balance. Because the heat capacity of the porous medium depends on the fluid saturations, there is coupling between the heat balance and the saturation equations. Although this coupling is weak, Shutler takes it into account. Because fluid saturations are constant at the SCF, he finds that its velocity is constant as well. The steam zone is considered as a zone of constant high temperature in which oil, non-condensing gas (steam) and connate water are present. In the downstream cold zone oil and water are present at the original reservoir temperature. Capillary forces are disregarded. Water and oil conservation equations applied at the SCF, combined with the Buckley–Leverett equation for gas/oil in the steam zone and for oil/water in the cold zone, lead to a complete solution of the model equations. However, the assumption that the steam zone contains connate water only is not clear. This assumption is apparently necessary to close the problem. It may also have an undesirable effect on the prediction of the efficiency of the steamdrive process. Models related to the one of Shutler have been proposed by Pope [24] and Yortsos [33].

Wingard and Orr [32] extended the model of Shutler to incorporate three phase flow in the steam zone. A careful inspection of their paper led us to the conclusion that the presented model cannot be used for our set of parameter values. To be precise, the upstream saturations at the SCF cannot be obtained from the upstream boundary conditions by integrating the mass balance equations. We need additional conditions at the SCF to obtain a unique solution. From a physical point of view, such conditions should originate from a detailed local model of the steam condensation process itself.

The one-dimensional steamdrive model considered in this paper unifies a hyperbolic interface model and a parabolic transition model. In the hyperbolic setting, a SCF exists and moves at a given speed through the porous medium. It separates the hot steam and the cold liquid regions. All steam condenses at the SCF and no capillary forces are present. Inspired by the work of Stewart and Udell [29], Udell [31] and Menegus and Udell [22], we consider various local transition models. In these models, steam condenses according to a delta distribution at the SCF and fluid flow towards and from the SCF is governed by Darcy's law including capillary effects. The model equations in the transition zone are solved by the method of matched asymptotic expansions. This leads to solutions in the form of traveling waves, moving with the speed of the SCF. The conditions for such waves to exist are precisely the missing matching conditions for the saturations at the SCF. We will explicitly show how different transition models yield different saturation combinations at the SCF and, consequently, different solutions of the hyperbolic model. These differences are not always small.

For instance, when comparing the results of a transition model with constant capillary diffusion and one with Brooks–Corey three phase capillary pressures, the differences are well-noticeable and cannot be disregarded for practical purposes.

Such dependence on details of the transition model (i.e., parabolic regularization) is known to occur in systems of conservation laws. It arises in the context of transitional waves, as discussed by Isaacson et al. [15,16], Guzmán and Fayers [13] and Glimm [9]. Using vanishing viscosity (in our case vanishing capillary diffusion and heat conduction) as the entropy condition for the hyperbolic system, one finds traveling waves describing the transition through the shock. If the traveling wave con-

Table 1
Summary of physical input parameters.[1]

| Physical quantity | Symbol | Value | Unit |
|---|---|---|---|
| characteristic length | $L$ | 100 | [m] |
| steam temperature | $T_1$ | 486 | [K] |
| reservoir temperature | $T_0$ | 313 | [K] |
| injection rate steam | $u_{\text{inj}}$ | $9.52 \cdot 10^{-4}$ | $[\text{m}^3/\text{m}^2/\text{s}]$ |
| steam viscosity | $\mu_{\text{g}}$ | $1.63 \cdot 10^{-5}$ | [Pa s] |
| oil viscosity at $T_1$ | $\mu_{\text{o}}(T_1)$ | $2.45 \cdot 10^{-3}$ | [Pa s] |
| oil viscosity at $T_0$ | $\mu_{\text{o}}(T_0)$ | 0.180 | [Pa s] |
| water viscosity at $T_1$ | $\mu_{\text{w}}(T_1)$ | $1.30 \cdot 10^{-4}$ | [Pa s] |
| water viscosity at $T_0$ | $\mu_{\text{w}}(T_0)$ | $7.21 \cdot 10^{-4}$ | [Pa s] |
| viscosity $\ln \mu_i/\mu_{\text{r}} = a_i + b_i/T$ | $\mu_i$ | $\mu_i(T)$ | [Pa s] |
| reference viscosity | $\mu_{\text{r}}$ | 1 | [Pa s] |
| coefficient in oil viscosity | $a_{\text{o}}$ | $-13.79$ | [–] |
| coefficient in oil viscosity | $b_{\text{o}}$ | 3781 | [K] |
| coefficient in water viscosity | $a_{\text{w}}$ | $-12.06$ | [–] |
| coefficient in oil viscosity | $b_{\text{w}}$ | 1509 | [K] |
| Brooks–Corey sorting factor | $\lambda_{\text{s}}$ | 2 | [–] |
| enthalpy $\text{H}_2\text{O}(l)(T_0) \rightarrow \text{H}_2\text{O}(g)(T_1)$ | $\Delta H$ | 2636 | [kJ/kg] |
| effective heat capacity of rock | $(\rho c)_{\text{r}}$ | 2029 | $[\text{kJ}/\text{m}^3/\text{K}]$ |
| thermal coefficient in (2.14) | $\alpha$ | 0.017 | [–] |
| capillary diffusion constant | $D$ | $2.2 \cdot 10^{-7}$ | $[\text{m}^2/\text{s}]$ |
| velocity SCF | $v_{\text{st}}$ | $7.12 \cdot 10^{-5}$ | [m/s] |
| porosity | $\phi$ | 0.38 | $[\text{m}^3/\text{m}^3]$ |
| permeability | $k$ | $4.3 \cdot 10^{-13}$ | $[\text{m}^2]$ |
| interfacial tension | $\sigma$ | $30 \cdot 10^{-3}$ | [N/m] |
| water density | $\rho_{\text{w}}$ | 1000 | $[\text{kg}/\text{m}^3]$ |
| steam density | $\rho_{\text{g}}$ | 10.2 | $[\text{kg}/\text{m}^3]$ |
| connate water saturation | $S_{\text{wc}}$ | 0.15 | $[\text{m}^3/\text{m}^3]$ |
| residual gas saturation | $S_{\text{gr}}$ | 0.0 | $[\text{m}^3/\text{m}^3]$ |
| residual oil saturation | $S_{\text{or}}$ | 0.0 | $[\text{m}^3/\text{m}^3]$ |

[1] The values of the steam parameters in table 1 assume a steam pressure of 20 bar. Furthermore, the value of the thermal coefficient $\alpha$ is based on a thermal diffusivity of $9.85 \cdot 10^{-7}$ $[\text{m}^2/\text{s}]$. Note that this coefficient is proportional to the ratio of the capillary and thermal diffusivity.

Table 2
Expressions for relative permeabilities.

| Symbol | Quantity | Expression |
|---|---|---|
| $k_{\mathrm{rw}}$ | water permeability | $((S_{\mathrm{w}} - S_{\mathrm{wc}})/(1 - S_{\mathrm{wc}}))^4$ |
| $k_{\mathrm{ro}}$ | oil permeability | $(S_{\mathrm{o}}/(1 - S_{\mathrm{wc}}))^4$ |
| $k_{\mathrm{rg}}$ | steam permeability | $(S_{\mathrm{g}}/(1 - S_{\mathrm{wc}}))^4$ |

nects a node and a saddle (of the associated dynamical system), the resulting shock is admissible as a Lax shock, see Isaacson et al. [15,16]. If, however, the traveling wave connects two saddles, the Lax criteria fail. But the resulting shock is still admissible in the physical sense. It is called a transitional shock wave. Saddle to saddle connections are sensitive to perturbations of the system. This explains in an unspecified way the dependence of the matching conditions at the SCF on the parameters of the transition model.

In section 2 we describe the physical model. First we present the base case, with input parameters summarized in tables 1 and 2. In the base case we model the transition region with constant (saturation independent) capillary diffusion, an abrupt temperature drop from steam temperature to reservoir temperature at the SCF and no steam downstream of the SCF. We also study three cases in which one of these simplifying conditions is relaxed: (i) Brooks–Corey three-phase capillary pressures, (ii) an exponential temperature decline downstream of the SCF, and (iii) a non-zero steam saturation downstream of the SCF in the transition region. In section 3 we present the analysis of the base case. In section 4 we analyze the problem with different transition models. In particular, we compare the results of the three cases defined in section 2 with the base case. In section 5 we study the variation of model parameters. There we introduce the average oil saturation in the steam zone and investigate its dependence on reservoir and fluid properties. To construct the full solution of the steamdrive problem is rather involved. Therefore we present in section 5 an approximation, which is fairly straightforward to obtain. In figure 13 we compare the results for the full solution and this approximation. It clearly indicates in which parameter range the approximation is acceptable for engineering purposes. We summarize our findings in section 6, which contains the conclusions.

## 2. Physical model

Oil displacement by steamdrive through a porous medium is a complex physical process which is controlled by the steam condensation process and by viscous and capillary forces; see, for instance, Wingard and Orr [32] or Stewart and Udell [29]. In this paper we propose a simplified approach in which all steam condenses at an a priori known Steam Condensation Front (SCF) and in which capillary forces as well as temperature variations are disregarded except in a small neighborhood of that front. Here “small” must be understood in a suitable dimensionless context. To model this,

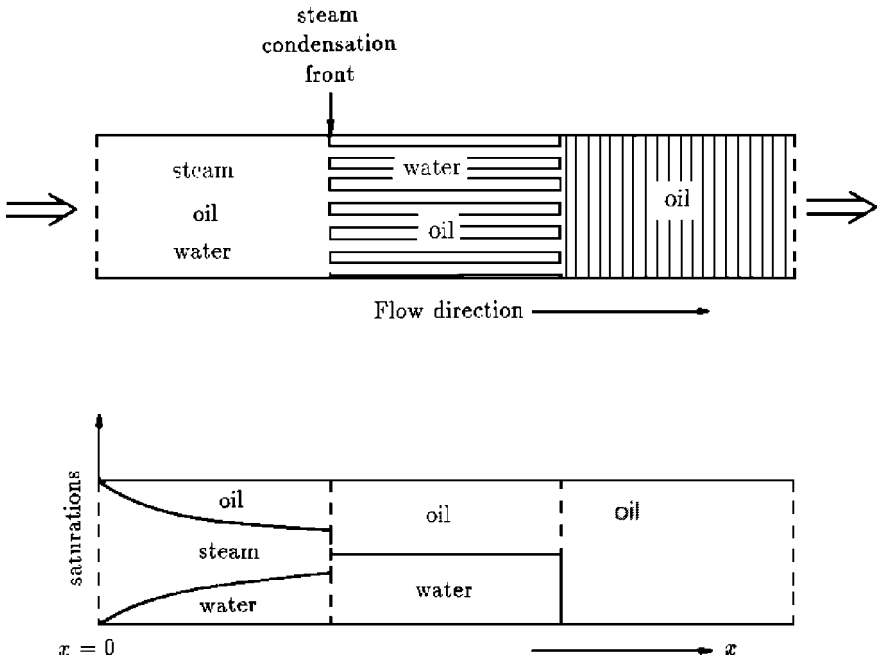


Figure 1. Sketch of the one-dimensional steam displacement process and the phase saturations.

we consider a global *interface model* in which capillary forces are absent on any scale and in which the interface (SCF) separates the hot steam zone from the remainder of the reservoir. Further we consider a local *transition model* which takes capillary forces and temperature variations into account at the SCF. The transition model yields the correct matching conditions at the SCF in the hyperbolic interface model.

In modeling a one-dimensional flood through a reservoir we consider the porous medium to be homogeneous, with constant porosity $\phi$, and of semi-infinite extent. The multi-phase flow (oil, water, steam (gas)) through the reservoir is directed in what we choose to be the positive $x$-axis. Hence the phase saturations $S_{\rm o}$, $S_{\rm w}$, and $S_{\rm g}$ are functions of position $x$ and time $t$ only, see figure 1. Initially, at $t = 0$, the reservoir contains oil and connate water: thus, for all $x > 0$

$$S_{\rm o}(x,0) = 1 - S_{\rm wc}, \qquad S_{\rm w}(x,0) = S_{\rm wc}, \qquad S_{\rm g}(x,0) = 0. \tag{2.1}$$

From the left steam of 100% quality is injected at rate $u_{\rm inj}$: thus, at $x = 0$ and for all $t > 0$

$$S_{\rm o}(0,t) = 0, \qquad S_{\rm w}(0,t) = S_{\rm wc}, \qquad S_{\rm g}(0,t) = 1 - S_{\rm wc}. \tag{2.2}$$

In writing these initial and boundary conditions we assume that the residual oil and gas saturations are constant. Without loss of generality they are given the value zero: see also table 1, where the values of all quantities used throughout this paper are given.

Oil and water are produced at the right, in our simplified model at $x = \infty$. All fluids, also steam, are considered incompressible. To avoid non-essential complications

the thermal expansion coefficients of the fluids are taken to be zero. Heat losses to the surroundings as well as gravity effects are not considered. Furthermore, we assume that the oil is non-distillable: the partial vapor pressure of the oil in the gas phase is negligible. Consequently, we ignore the presence of a distillable oil bank.

### *2.1. Interface model*

As in figure 1, we distinguish two zones: one upstream and one downstream relative to the SCF. *Upstream* is the steam zone. We assume that this zone is at constant steam temperature $T_1$, thus disregarding the temperature gradient as a consequence of the pressure gradient driving the fluids and the boiling point curve. Capillary forces are neglected and fluid transport is governed by Darcy's law for multi-phase flow. With the exception of section 5, we use power law expressions for the relative permeabilities. In this work we keep the exponents fixed and all equal to 4, see table 2. Any other choice greater than 1 would give the same qualitative results. *Downstream* is the liquid zone, where only oil and water are present. This zone is at constant reservoir temperature $T_0$. Again capillary forces are disregarded and fluid transport is governed by Darcy's law for multi-phase flow. The relative permeabilities are the same as in the steam zone.

Because oil and water experience different temperatures, their viscosities $\mu_{i=\mathrm{o,w}}$ may vary substantially. To account for this we take the well-known expressions (see Reid et al. [26] and table 1)

$$\ln \frac{\mu_i}{\mu_{\mathrm{r}}} = a_i + \frac{b_i}{T}, \quad i = \mathrm{o}, \mathrm{w}. \tag{2.3}$$

The two zones are separated by the SCF. The velocity of this front $v_{\mathrm{st}}$ is determined from a local heat balance, in which the heat released by the condensing steam impinging on the SCF is equal to the amount of heat necessary to warm up the reservoir, see Mandl and Volek [20]. The result is

$$v_{\mathrm{st}} = \frac{\rho_{\mathrm{g}} \Delta H u_{\mathrm{inj}}}{(\rho c)_{\mathrm{r}} (T_1 - T_0)}. \tag{2.4}$$

The symbols appearing in this expression are explained in table 1. The effective heat capacity of the reservoir includes the heat capacity of the matrix and the fluids in the pores. Variations in saturations have a relatively small effect on the effective heat capacity. This allows us to decouple the balance equations for heat and for mass. Therefore we may consider the velocity of the SCF as given.

In the interface approach the steam condenses at the SCF, $x = v_{\mathrm{st}} t$, only. Due to condensation there occurs water production $Q_{\mathrm{w}}$ [$\mathrm{m}^3/(\mathrm{m}^3\ \mathrm{s})$] (volume of produced water due to condensation per unit volume reservoir and per unit time) according to

$$Q_{\mathrm{w}} = \frac{\rho_{\mathrm{g}}}{\rho_{\mathrm{w}}} r \delta(x - v_{\mathrm{st}} t), \tag{2.5}$$

and steam loss $Q_{\mathrm{g}}$ [$\mathrm{m}^3/(\mathrm{m}^3\ \mathrm{s})$] (the volume of condensed steam per unit volume of reservoir per unit time) according to

$$Q_{\mathrm{g}} = r\delta(x - v_{\mathrm{st}}t). \tag{2.6}$$

Here $\delta()$ $[1/\mathrm{m}]$ denotes the Dirac distribution and $r$ $[\mathrm{m}/\mathrm{s}]$ the a priori unknown steam condensation rate. This factor has to be determined from the saturations at the SCF. In the absence of heat losses it does not depend on the location of the SCF. Using the values of the parameters in table 1, we find only a weak dependence of $r$ on the saturations. Computations show that $r$ is almost equal to the steam injection rate, see section 3.3.

In order to match saturations across the SCF we need to make a detailed analysis of the possible transitions occurring there. For this we need a model which is outlined below.

### *2.2. Transition model*

In the transition model we regularize the (possible) discontinuous saturations at the SCF by incorporating capillary effects. In addition we have to specify the condensation process as well as the temperature variation within the transition region. We shall first formulate a simple base case to illustrate the underlying ideas and then define three extensions.

#### *2.2.1. Base case*

Here we assume that the effect of capillary forces can be described in terms of a constant diffusivity $D$. In section 3.2 we let $D \downarrow 0$ in the appropriate dimensionless setting (in fact $D/Lu_{\mathrm{inj}} \downarrow 0$), which yields the missing matching conditions at the SCF. When $D/Lu_{\mathrm{inj}}$ is small, we have a small transition region which is centered at the SCF and which travels with the same velocity, see figure 2. To study the saturations within the transition region we introduce the dimensionless variable

$$\xi = \frac{x - v_{\mathrm{st}}t}{L}\,\frac{Lu_{\mathrm{inj}}}{D} \tag{2.7}$$

and consider the blow-up as $D/Lu_{\mathrm{inj}} \downarrow 0$. In terms of $\xi$ this yields a transition region extending from $\xi = -\infty$ to $\xi = +\infty$. The corresponding limit saturations have the form of traveling waves. As $\xi \to -\infty$ the waves have to be matched with the outer saturations in the steam (hot) zone and as $\xi \to +\infty$ with the outer saturations in the liquid (cold) zone.

For simplicity we assume that also in the transition region the steam condenses at the SCF, where $\xi = 0$. This means that we ignore mechanisms causing a delay of the steam condensation process. Consequently two transition sub-regions can be

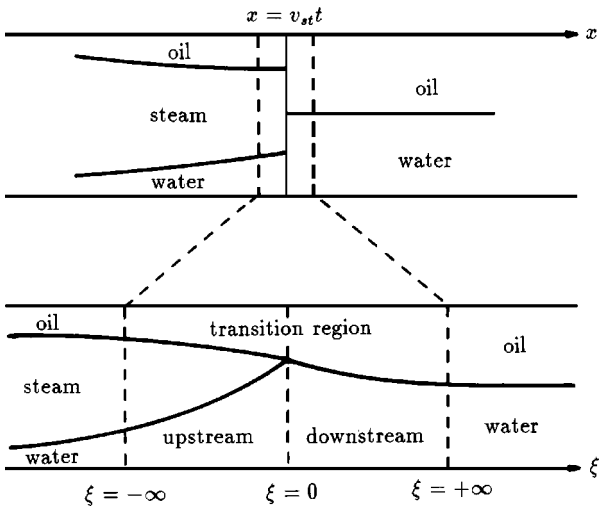


Figure 2. Sketch of transition region between the steam zone and the cold zone. The transition region consists of the SCF, an upstream region with steam of constant temperature and a downstream region. In the base case, the downstream region has the cold reservoir temperature and no steam is present there. Possible extensions are discussed in sections 2.2.2–2.2.4.

identified: one upstream and one downstream of the SCF. In both sub-regions we assume again that the temperature is constant: i.e.,

$$T(\xi) = \begin{cases} T_1 & \text{for } \xi < 0, \\ T_0 & \text{for } \xi > 0. \end{cases} \tag{2.8}$$

We use this expression in the viscosity formula (2.3) to account for the temperature change in the transition region. Expression (2.8) describes the case where the temperature changes at a much smaller scale than the saturations. The case where temperature and saturations change at similar scales is considered in section 2.2.3. The assumption of local thermodynamic equilibrium ($T_0$ is much smaller than the boiling temperature) means that no steam can be present in the downstream part of the transition zone. In particular, it implies

$$S_{\mathrm{g}}(\xi = 0) = 0. \tag{2.9}$$

It turns out that this condition is also needed to obtain a unique set of matching conditions at the SCF in the interface model. However, we will investigate cases where $S_{\mathrm{g}}(0) > 0$ as well.

*2.2.2. Brooks–Corey capillary pressure diffusion*

In this extension of the base case we keep (2.8) and (2.9) but we take the capillary forces into account more realistically. Clearly, this involves the introduction of three phase capillary pressures. Since experimental data are hardly available, we assume that the oil–water capillary pressure $p_{\mathrm{o}} - p_{\mathrm{w}}$ only depends on the water saturation and the

steam–oil capillary pressure $p_g - p_o$ only on the steam saturation (Aziz and Settari [1]). Combining these pressures an expression results for the steam–water capillary pressure $p_g - p_w$. Thus in this approach, three phase capillary pressures can be expressed in terms of well-known two phase capillary pressures. The saturation dependence of the capillary pressures enters through the Leverett functions. We write

$$P_c^{ow} = \sigma\sqrt{\frac{\phi}{k}}J^{ow}(S_w) \quad \text{and} \quad P_c^{go} = \sigma\sqrt{\frac{\phi}{k}}J^{go}(S_g), \tag{2.10}$$

where we have used the fact that the interfacial tension ($\sigma$) between oil and water and between gas and oil is approximately the same. For the Leverett functions we use the empirical Brooks–Corey expressions (Dullien [5]). This means that $J^{ow}$ is proportional to

$$\left(\frac{S_w - S_{wc}}{1 - S_{wc}}\right)^{-1/\lambda_s}, \tag{2.11}$$

where $\lambda_s$ is a factor related to the sorting. The expression for $J^{go}$ is obtained by substituting $S_w = 1 - S_g$ into (2.11).

When $\lambda_s$ is large, the capillary pressure curve is flat, meaning that the grains have approximately the same size and are well sorted. When $\lambda_s$ is small, the capillary pressure curve is steep, and the grains are badly sorted. Finally, we assume that the Leverett function satisfies $J(1/2) = 1/2$. For most experimental data, as in [5], indeed $0.3 < J(1/2) < 0.7$. All of this leads to the following expressions for the capillary pressure:

$$P_c^{ow}(S_w) = \frac{\sigma}{2}\sqrt{\frac{\phi}{k}}\left(\frac{1/2 - S_{wc}}{1 - S_{wc}}\right)^{1/\lambda_s}\left(\frac{S_w - S_{wc}}{1 - S_{wc}}\right)^{-1/\lambda_s}$$

and (2.12)

$$P_c^{go}(S_g) = P_c^{ow}(1 - S_g).$$

In section 4 we introduce the capillary pressure functions in the different equations. This leads to terms resembling non-linear diffusion. As a characteristic capillary diffusion number we find

$$D = \frac{\sigma\sqrt{\phi k}}{\mu_o}. \tag{2.13}$$

As in the base case we investigate the process $D/Lu_{inj} \downarrow 0$ to obtain matching conditions for the interface model.

*2.2.3. Temperature variation*

Here we consider constant capillary diffusion and (2.9), but we modify (2.8). To model the temperature distribution properly, one must consider the heat-balance equation in terms of the local coordinate $\xi$ and construct a solution satisfying $T \to T_1$ as $\xi \to -\infty$ and $T \to T_0$ as $\xi \to +\infty$. This procedure may be complicated because

the coefficients in the temperature equation depend on the fluid saturations. Ignoring this dependence, Miller [23] finds a solution of the form

$$T(\xi) = \begin{cases} T_1 & \text{for } \xi < 0, \\ T_0 + (T_1 - T_0)\mathrm{e}^{-\alpha\xi} & \text{for } \xi > 0. \end{cases} \tag{2.14}$$

Here the constant $\alpha$ is the ratio of the front velocity and the thermal conductivity in the appropriate dimensionless setting.

*2.2.4. Positive steam saturation at SCF*

Now we consider a constant capillary diffusivity and (2.8), but we modify (2.9). If we drop the assumption concerning local thermodynamic equilibrium, there is no physical reason why (2.9) should hold. In that case, steam condenses at a rate which is limited by diffusive processes in the vapor zone. Corresponding to this we construct solutions for which steam is also present in the downstream region. To obtain such solutions we have to prescribe a positive value for the steam saturation at the SCF:

$$S_{\mathrm{g}}(\xi = 0) > 0 \quad \text{(prescribed)}. \tag{2.15}$$

*Remark.* In section 5 we discuss the results of computations for the full Brooks–Corey case. There we keep (2.8) and (2.9) in the transition model, but we modify both the capillary pressure and relative permeabilities according to Brooks–Corey and Corey–Stone expressions. This is a modification of section 2.2.2 in the sense that power law relative permeabilities are replaced by the Corey–Stone relative permeabilities, where $k_{\mathrm{rw}} = k_{\mathrm{rw}}(S_{\mathrm{w}}), k_{\mathrm{rg}} = k_{\mathrm{rg}}(S_{\mathrm{g}})$ and $k_{\mathrm{ro}} = k_{\mathrm{ro}}(S_{\mathrm{w}}, S_{\mathrm{g}})$.

## 3. Mathematical formulation of base case

### *3.1. Interface model*

The interface model described in section 2.1 results in the following mass balance equations (Falls and Schulte [6]):

$$\phi\frac{\partial S_{\mathrm{w}}}{\partial t} + \frac{\partial u f_{\mathrm{w}}}{\partial x} = Q_{\mathrm{w}} = \frac{\rho_{\mathrm{g}}}{\rho_{\mathrm{w}}} r\delta(x - v_{\mathrm{st}}t), \tag{3.1}$$

$$\phi\frac{\partial S_{\mathrm{g}}}{\partial t} + \frac{\partial u f_{\mathrm{g}}}{\partial x} = -Q_{\mathrm{g}} = -r\delta(x - v_{\mathrm{st}}t), \tag{3.2}$$

$$\phi\frac{\partial S_{\mathrm{o}}}{\partial t} + \frac{\partial u f_{\mathrm{o}}}{\partial x} = 0. \tag{3.3}$$

The non-zero terms in the right side of equations (3.1) and (3.2) are a consequence of the steam condensation at the SCF, see also expressions (2.5) and (2.6). Except for these terms, system (3.1)–(3.3) consists of the standard multi-phase flow equations in

which $u$ denotes the total specific discharge and $f_i$ ($i = \mathrm{o}, \mathrm{w}, \mathrm{g}$) the fractional flow functions

$$f_i = \frac{M_{\mathrm{o}i} k_{\mathrm{r}i}}{M_{\mathrm{ow}} k_{\mathrm{rw}} + k_{\mathrm{ro}} + M_{\mathrm{og}} k_{\mathrm{rg}}}, \tag{3.4}$$

where $M_{\mathrm{o}i}$ are the mobility ratios

$$M_{\mathrm{o}i} = \frac{\mu_{\mathrm{o}}}{\mu_i}. \tag{3.5}$$

Note that these quantities have different values up- and downstream of the SCF. This is due to the temperature dependence of the viscosity, which enters through equations (2.3). In the interface model we will not write this dependence explicitly. Furthermore, note that the specific discharge $u$ and the steam condensation rate $r$ are both unknown and have to be determined from the problem. However, by adding equations (3.1)–(3.3) and using $\sum S_i = \sum f_i = 1$, we find the volume balance

$$\frac{\partial u}{\partial x} = -r\left(1 - \frac{\rho_{\mathrm{g}}}{\rho_{\mathrm{w}}}\right)\delta(x - v_{\mathrm{st}}t).$$

Applying the boundary condition $u(0,t) = u_{\mathrm{inj}}$ (steam injection rate), we find upon integration

$$u = u(x,t) = u_{\mathrm{inj}} - r\left(1 - \frac{\rho_{\mathrm{g}}}{\rho_{\mathrm{w}}}\right)H(x - v_{\mathrm{st}}t), \tag{3.6}$$

where $H$ denotes the Heaviside function: $H(s) = 0$ for $s < 0$ and $H(s) = 1$ for $s > 0$. Thus the phase saturations and the constant $r$ have to be determined from equations (3.1)–(3.3), (3.6) and the initial-boundary conditions (2.1), (2.2).

Next we rewrite the equations in dimensionless form by redefining

$$S_{\mathrm{w}} := \frac{S_{\mathrm{w}} - S_{\mathrm{wc}}}{1 - S_{\mathrm{wc}}}, \qquad S_{\mathrm{o}} := \frac{S_{\mathrm{o}}}{1 - S_{\mathrm{wc}}}, \qquad S_{\mathrm{g}} := \frac{S_{\mathrm{g}}}{1 - S_{\mathrm{wc}}},$$
$$t := \frac{u_{\mathrm{inj}} t}{\phi L}, \qquad u := \frac{u}{u_{\mathrm{inj}}}, \qquad x := \frac{x}{L},$$

and by introducing the dimensionless steam condensation rate

$$\Lambda = \frac{r}{u_{\mathrm{inj}}} \tag{3.7}$$

and the dimensionless SCF velocity

$$v = \frac{v_{\mathrm{st}}}{u_{\mathrm{inj}}}\phi(1 - S_{\mathrm{wc}}). \tag{3.8}$$

Eliminating the oil saturation by setting $S_{\mathrm{o}} = 1 - S_{\mathrm{w}} - S_{\mathrm{g}}$, we obtain the steamdrive problem

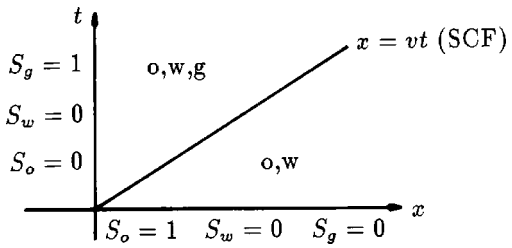


Figure 3. Distribution of phases in the $x, t$-plane.

**Problem SD.** Find the phase saturations $S_{\mathrm{w}}$, $S_{\mathrm{g}}$ and the condensation constant $\Lambda$ such that

$$\frac{\partial S_{\mathrm{w}}}{\partial t} + \frac{\partial u f_{\mathrm{w}}}{\partial x} = \frac{\rho_{\mathrm{g}}}{\rho_{\mathrm{w}}} \Lambda \delta(x - vt), \tag{3.9}$$

$$\frac{\partial S_{\mathrm{g}}}{\partial t} + \frac{\partial u f_{\mathrm{g}}}{\partial x} = -\Lambda \delta(x - vt), \tag{3.10}$$

and

$$u = 1 - \Lambda \left( 1 - \frac{\rho_{\mathrm{g}}}{\rho_{\mathrm{w}}} \right) H(x - vt), \tag{3.11}$$

for $x > 0$ and $t > 0$, subject to initial–boundary conditions

$$S_{\mathrm{w}}(x, 0) = 0, \quad S_{\mathrm{g}}(x, 0) = 0 \quad \text{for all } x > 0, \tag{3.12}$$

and

$$S_{\mathrm{w}}(0, t) = 0, \quad S_{\mathrm{g}}(0, t) = 1 \quad \text{for all } t > 0. \tag{3.13}$$

We shall consider solutions of this problem for which no steam is present in the downstream region: i.e., we pose the additional condition (as part of problem SD)

$$S_{\mathrm{g}}(x, t) = 0 \quad \text{for } x > vt, \ t > 0. \tag{3.14}$$

This seems a natural condition since the temperature in this region is the cold reservoir temperature $T_0$ at which no steam can survive at the current reservoir pressure. In figure 3 we show the regions in which the various phases are present.

In analyzing problem SD, we shall frequently represent (part of) the solution in the $(S_{\mathrm{w}}, S_{\mathrm{g}})$ plane (phase plane). Since $0 \leqslant S_{\mathrm{w}} + S_{\mathrm{g}} = 1 - S_{\mathrm{o}} \leqslant 1$, the solution is confined to the closed triangular domain $\mathcal{D}$ in figure 4. The vertices are denoted by $O = (0, 0)$, $T = (0, 1)$ and $A = (1, 0)$. Note that any solution must pass through the points $T$ (boundary conditions) and $O$ (initial conditions), and must coincide with part of the $S_{\mathrm{w}}$-axis (solution in the cold zone where $S_{\mathrm{g}} = 0$).

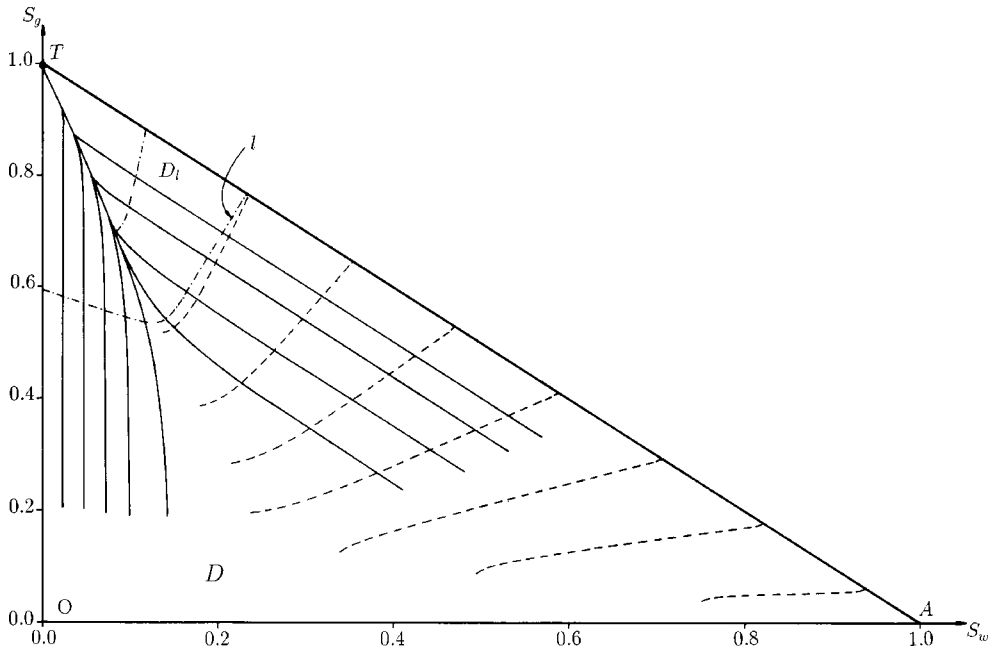


Figure 4. Slow (dashed) and fast (solid) rarefactions, see (3.23). The eigenvalues of the slow rarefactions increase from the right to the left and the eigenvalues of the fast rarefactions increase from the top to the bottom.

In the steam zone $x < vt$, where the three phases are present and where $u = 1$ (see equation (3.11)), we have to solve (3.9) and (3.10), which we write in vector notation as

$$\frac{\partial \mathbf{S}}{\partial t} + \frac{\partial}{\partial x}\mathbf{f}(\mathbf{S}) = \mathbf{0}. \tag{3.15}$$

Here $\mathbf{S}$ and $\mathbf{f}$ denote the column vectors $\mathbf{S} = (S_{\mathrm{w}}, S_{\mathrm{g}})^{\mathrm{T}}$ and $\mathbf{f} = (f_{\mathrm{w}}, f_{\mathrm{g}})^{\mathrm{T}}$. The eigenvalues $\lambda_1$ and $\lambda_2$ of the Jacobian matrix

$$D\mathbf{f} = \begin{pmatrix} f_{\mathrm{ww}} & f_{\mathrm{wg}} \\ f_{\mathrm{gw}} & f_{\mathrm{gg}} \end{pmatrix}, \tag{3.16}$$

where $f_{ij} = \partial f_i / \partial S_j$ $(i, j = \mathrm{w}, \mathrm{g})$, are given by

$$\lambda_{\mathrm{k}}(\mathbf{S}) = \frac{1}{2}(f_{\mathrm{ww}} + f_{\mathrm{gg}}) + (-1)^k \frac{1}{2}\sqrt{\{(f_{\mathrm{ww}} - f_{\mathrm{gg}})^2 + 4 f_{\mathrm{wg}} f_{\mathrm{gw}}\}}. \tag{3.17}$$

Because we used Corey type relative permeabilities, as in table 2, the eigenvalues are real for all saturations in $\mathcal{D}$. Moreover, the system is strictly hyperbolic, with $0 \leqslant \lambda_1 < \lambda_2$, except at four points: the three vertices and one interior point. These are the umbilic points, see Marchesin et al. [21] and Guzmán and Fayers [12]. There the eigenvalues are equal and the hyperbolic system degenerates. Due to the high

mobility contrast, the interior umbilic point is close to $O$ and plays no role in the analysis.

The right eigenvectors of $D\mathbf{f}$ are denoted by $\mathbf{t}_k = \mathbf{t}_k(\mathbf{S})$, $k = 1, 2$. A solution of (3.15), satisfying constant boundary conditions, consists in general of a combination of shock waves, constant states and rarefaction waves (Lax [18], LeVeque [19], Smoller [28], Hellferich [14]). Rarefaction waves are self-similar solutions depending on $\eta = x/t$ only. Considering $\mathbf{S} = \mathbf{S}(\eta)$, we find from (3.15) that they satisfy

$$-\eta \frac{\mathrm{d}\mathbf{S}}{\mathrm{d}\eta} + \frac{\mathrm{d}}{\mathrm{d}\eta}\mathbf{f}(\mathbf{S}) = \mathbf{0} \tag{3.18}$$

or

$$-\eta \frac{\mathrm{d}\mathbf{S}}{\mathrm{d}\eta} + D\mathbf{f}\frac{\mathrm{d}\mathbf{S}}{\mathrm{d}\eta} = 0, \tag{3.19}$$

in which we recognize an eigenvalue problem for the matrix $D\mathbf{f}$. Hence,

$$\frac{\mathrm{d}\mathbf{S}}{\mathrm{d}\eta} = \alpha(\eta)\mathbf{t}_k(\mathbf{S}) \tag{3.20}$$

and

$$\eta = \lambda_k(\mathbf{S}), \tag{3.21}$$

where $\alpha$ is an $\eta$-dependent proportionality factor which is a priori unknown. As a consequence of (3.21) we observe that a rarefaction wave is only possible if the eigenvalue varies monotonically along its representation in the phase plane. Differentiating (3.21) with respect to $\eta$ and using (3.20) gives

$$1 = \nabla\lambda_k(\mathbf{S}) \cdot \frac{\mathrm{d}\mathbf{S}}{\mathrm{d}\eta} = \alpha(\eta)\nabla\lambda_k(\mathbf{S}) \cdot \mathbf{t}_k(\mathbf{S}), \tag{3.22}$$

where $\nabla$ denotes the gradient in the phase plane. Substituting this into (3.20) yields the system

$$\frac{\mathrm{d}\mathbf{S}}{\mathrm{d}\eta} = \frac{1}{\nabla\lambda_k(\mathbf{S}) \cdot \mathbf{t}_k(\mathbf{S})}\mathbf{t}_k(\mathbf{S}), \tag{3.23}$$

as long as $\nabla\lambda_k(\mathbf{S}) \cdot \mathbf{t}_k(\mathbf{S}) \neq 0$ (genuine nonlinearity, Lax [18]).

If a rarefaction is to be part of the solution of problem SD we obviously want

$$\lambda_2(\mathbf{S}) \leqslant v, \tag{3.24}$$

since otherwise the rarefaction would exceed the SCF, yielding a multi-valued solution. The region where (3.24) holds strictly is indicated in figure 4 as the set $\mathcal{D}_l$ above the curve

$$l = \big\{(S_{\mathrm{w}}, S_{\mathrm{g}}):\ \lambda_2(S_{\mathrm{w}}, S_{\mathrm{g}}) = v\big\}. \tag{3.25}$$

In spite of (3.24) we computed solutions of the system (3.23) in the full triangular domain $\mathcal{D}$. Though not strictly necessary for the analysis presented here, this gives a clear picture of the slow and fast rarefaction waves in the $S_{\mathrm{w}}$–$S_{\mathrm{g}}$ phase plane. For $k = 2$, the fast rarefactions, we solved (3.23) for $\eta < v$ and for $\eta > v$ with initial values $(S_{\mathrm{w}}(v), S_{\mathrm{g}}(v)) \in l$. Computing the orbits backwards in $\eta$ we found that they all reached the top $T$, i.e., the boundary conditions, at $\eta = 0$: see figure 4, where several of these fast rarefactions are shown (solid curves). The degenerate behavior of the right hand side of equations (3.23) causes the collapse of the orbits in the top of the triangle. This is discussed in detail by Marchesin et al. [21].

For $k = 1$, the slow rarefactions, we solved (3.23) forwards in $\eta$ with initial values taken from the segment $AT$. The corresponding start value of $\eta$ is

$$\eta = \lambda_1(S_{\mathrm{w}}, S_{\mathrm{g}}) \quad \text{with } (S_{\mathrm{w}}, S_{\mathrm{g}}) \in AT. \tag{3.26}$$

These slow rarefactions are also shown in figure 4 (dashed curves). Both slow and fast rarefactions are shown up to points where the eigenvalues reach a local extremum (along the corresponding orbits). The curves connecting these points are part of the inflection locus, see Isaacson et al. [15].

We will not discuss the occurrence of shocks in the steam zone. Indeed, see region $\mathcal{D}_l$ in figure 4, the eigenvalues for the fast rarefactions increase from top to bottom and hence shocks do not arise for our choice of boundary conditions. To find a solution of problem SD we use only fast rarefactions or constant states upstream of the SCF. Later on, in section 3.3, where we discuss the matching conditions at the SCF, we show in fact that constant states are not allowed. Thus the solution for $x < vt$ consists of a fast rarefaction only. It connects the boundary condition $S_{\mathrm{g}} = 1$ to a point $(S_{\mathrm{w}}(v), S_{\mathrm{g}}(v)) \in l$ at the SCF.

If a pair $(S_{\mathrm{w}}^*, S_{\mathrm{g}}^*) \in AT$ represents a boundary condition different from (3.13), then the corresponding solution in the steam zone starts with a slow rarefaction (since $\lambda_1(S_{\mathrm{w}}^*, S_{\mathrm{g}}^*) = 0$), followed by a constant state, then followed by a fast rarefaction to match up with the SCF. This can only occur for boundary conditions above line $l$, provided the ensuing slow rarefaction does not intersect $l$ before transition to the fast path.

Next we turn to the cold region downstream of the SCF. Because of (3.14), only oil and water are present there. Hence we are left with the two phase Buckley–Leverett equation

$$\frac{\partial S_{\mathrm{w}}}{\partial t} + u^+ \frac{\partial f_{\mathrm{w}}}{\partial x} = 0 \quad \text{for } x > vt,\ t > 0, \tag{3.27}$$

where $u^+$ denotes the downstream velocity, see (3.11),

$$u^+ = 1 - \Lambda\left(1 - \frac{\rho_{\mathrm{g}}}{\rho_{\mathrm{w}}}\right). \tag{3.28}$$

We need to solve equation (3.27) with the a priori unknown saturation $S_{\mathrm{w}}^+ := \lim_{x \downarrow vt} S_{\mathrm{w}}(x, t)$ along the SCF and with $S_{\mathrm{w}} = 0$ initially. Assuming $S_{\mathrm{w}}^+$ to be constant

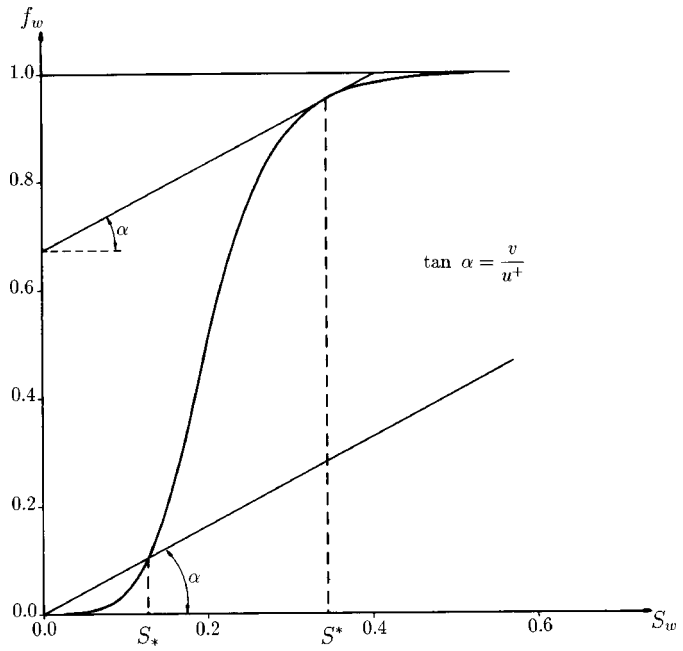


Figure 5. Construction of admissible $S_{\mathrm{w}}^+$ interval.

and using standard Buckley–Leverett theory, we find that the entropy solutions consist of shocks or rarefactions followed by shocks. Furthermore, only if the speed of the rarefactions or the shocks exceeds the speed of the SCF we find non-trivial solutions. With reference to figure 5 this implies that

$$S_* \leqslant S_{\mathrm{w}}^+ \leqslant S^* \quad \text{(non-trivial solutions)}, \tag{3.29}$$

where $S_*$ is the (smallest) root of

$$\frac{f_{\mathrm{w}}(S_w)}{S_w} = \frac{v}{u^+} \tag{3.30}$$

and $S^*$ is the largest root of

$$\frac{\mathrm{d}f_{\mathrm{w}}(S_w)}{\mathrm{d}S_{\mathrm{w}}} = \frac{v}{u^+}, \tag{3.31}$$

or

$$S_{\mathrm{w}}^+ = 0 \quad \text{(trivial solution)}. \tag{3.32}$$

The value $S_*$ corresponds to the smallest shock possible with speed $\geqslant v$, and $S^*$ corresponds to the largest rarefaction possible with speed $\geqslant v$.

Clearly, problem SD does not specify the saturations at the SCF. To find the physically correct matching condition, we need to consider the local behavior at the SCF by means of the transition model (see section 2.2.1). We shall use the notation

$$S_i^{+(-)} = \lim_{x\downarrow(\uparrow)vt} S_i(x,t), \quad i = \mathrm{g}, \mathrm{w}. \tag{3.33}$$

As a consequence of (3.14) we have $S_{\mathrm{g}}^{+} = 0$.

### 3.2. Transition model

In the transition model we include capillary forces in the form of a constant diffusivity $D$ in all three balance equations (3.1)–(3.3). As we shall show below, we can describe the behavior in the transition zone by the set of ordinary differential equations (3.48) and (3.49) in the upstream and downstream part of the transition zone respectively. To recast the equations in dimensionless form we proceed as in the previous section. Introducing in addition the dimensionless diffusivity

$$\varepsilon = \frac{D}{u_{\mathrm{inj}} L}, \tag{3.34}$$

we obtain for the water and steam saturations

$$\frac{\partial S_{\mathrm{w}}}{\partial t} + \frac{\partial u f_{\mathrm{w}}}{\partial x} = \frac{\rho_{\mathrm{g}}}{\rho_{\mathrm{w}}} \Lambda \delta(x - vt) + \varepsilon \frac{\partial^2 S_{\mathrm{w}}}{\partial x^2}, \tag{3.35}$$

$$\frac{\partial S_{\mathrm{g}}}{\partial t} + \frac{\partial u f_{\mathrm{g}}}{\partial x} = -\Lambda \delta(x - vt) + \varepsilon \frac{\partial^2 S_{\mathrm{g}}}{\partial x^2}, \tag{3.36}$$

where again $u$ and $\Lambda$ satisfy (3.11). Here $\varepsilon$ is a small number which we later send to zero. Using the values from table 1 we find as a typical value $\varepsilon = 2.31 \cdot 10^{-6}$.

Next, consider the stretched moving coordinate (see also (2.7))

$$\xi = \frac{x - vt}{\varepsilon}. \tag{3.37}$$

Regarding $S_{\mathrm{w}}$ and $S_{\mathrm{g}}$ as functions of $\xi$ and $t$, we find instead of (3.35) and (3.36) the equations

$$\varepsilon \frac{\partial S_{\mathrm{w}}}{\partial t} - v \frac{\partial S_{\mathrm{w}}}{\partial \xi} + \frac{\partial u f_{\mathrm{w}}}{\partial \xi} = \frac{\rho_{\mathrm{g}}}{\rho_{\mathrm{w}}} \Lambda \delta(\xi) + \frac{\partial^2 S_{\mathrm{w}}}{\partial \xi^2}, \tag{3.38}$$

$$\varepsilon \frac{\partial S_{\mathrm{g}}}{\partial t} - v \frac{\partial S_{\mathrm{g}}}{\partial \xi} + \frac{\partial u f_{\mathrm{g}}}{\partial \xi} = -\Lambda \delta(\xi) + \frac{\partial^2 S_{\mathrm{g}}}{\partial \xi^2}. \tag{3.39}$$

For $\varepsilon$ small, in fact letting $\varepsilon \downarrow 0$, we find to leading order

$$S_i(\xi, t) = S_i(\xi), \quad i = \mathrm{w}, \mathrm{g}, \tag{3.40}$$

where the traveling wave type transition saturations satisfy

$$-v\frac{\partial S_{\mathrm{w}}}{\partial \xi}+\frac{\partial u f_{\mathrm{w}}}{\partial \xi}=\frac{\rho_{\mathrm{g}}}{\rho_{\mathrm{w}}}\Lambda\delta(\xi)+\frac{\partial^2 S_{\mathrm{w}}}{\partial \xi^2}, \tag{3.41}$$

$$-v\frac{\partial S_{\mathrm{g}}}{\partial \xi}+\frac{\partial u f_{\mathrm{g}}}{\partial \xi}=-\Lambda\delta(\xi)+\frac{\partial^2 S_{\mathrm{g}}}{\partial \xi^2}, \tag{3.42}$$

for $-\infty<\xi<\infty$. These equations imply

$$-vS_{\mathrm{w}}+uf_{\mathrm{w}}=\frac{\rho_{\mathrm{g}}}{\rho_{\mathrm{w}}}\Lambda H(\xi)+\frac{\mathrm{d}S_{\mathrm{w}}}{\mathrm{d}\xi}+C_1, \tag{3.43}$$

$$-vS_{\mathrm{g}}+uf_{\mathrm{g}}=-\Lambda H(\xi)+\frac{\mathrm{d}S_{\mathrm{g}}}{\mathrm{d}\xi}+C_2, \tag{3.44}$$

where $C_1$ and $C_2$ are constants of integration. Because the base case temperature satisfies (2.8), we find that the water and oil viscosity and, hence, the mobility ratios $M_{\mathrm{ow}}$ and $M_{\mathrm{og}}$ have different values for $\xi>0$ and $\xi<0$. This means that the fractional flow functions in equations (3.43) and (3.44) also have a discontinuous $\xi$-dependence: $f_i=f_i^{\mathrm{r}}(S_{\mathrm{w}},S_{\mathrm{g}})$ for $\xi>0$ and $f_i=f_i^{\mathrm{l}}(S_{\mathrm{w}},S_{\mathrm{g}})$ for $\xi<0$.

We solve the transition saturation equations subject to the boundary conditions (3.33):

$$S_{\mathrm{w}}(-\infty)=S_{\mathrm{w}}^-,\qquad S_{\mathrm{g}}(-\infty)=S_{\mathrm{g}}^- \tag{3.45}$$

and

$$S_{\mathrm{w}}(+\infty)=S_{\mathrm{w}}^+,\qquad S_{\mathrm{g}}(+\infty)=0. \tag{3.46}$$

Letting $\xi\to\pm\infty$ in (3.43) and (3.44) yields the Rankine–Hugoniot condition

$$\text{(RH)}\quad \begin{cases} u^+f_{\mathrm{w}}^+-vS_{\mathrm{w}}^+=\dfrac{\rho_{\mathrm{g}}}{\rho_{\mathrm{w}}}\Lambda+f_{\mathrm{w}}^--vS_{\mathrm{w}}^-,\\ 0=-\Lambda+f_{\mathrm{g}}^--vS_{\mathrm{g}}^-, \end{cases} \tag{3.47}$$

where $f_i^-=f_i^{\mathrm{l}}(S_{\mathrm{w}}^-,S_{\mathrm{g}}^-)$, $f_{\mathrm{w}}^+=f_{\mathrm{w}}^{\mathrm{r}}(S_{\mathrm{w}}^+,S_{\mathrm{g}}^+)$ and $v$ the shock speed.

We will formulate conditions, in addition to (3.24), (3.29) and (3.47), which enable us to select a unique set of boundary values (3.45), (3.46). These conditions are related to the solvability of the boundary value problem (3.43)–(3.46). To investigate this we consider two sub-problems. Eliminating the constants $C_1$ and $C_2$ from equations (3.43) and (3.44), we consider for $\xi<0$ the boundary value problem

$$(P^l)\quad \begin{cases} \dfrac{\mathrm{d}S_{\mathrm{w}}}{\mathrm{d}\xi}=f_{\mathrm{w}}^{\mathrm{l}}-vS_{\mathrm{w}}-\big(f_{\mathrm{w}}^--vS_{\mathrm{w}}^-\big),\\ \dfrac{\mathrm{d}S_{\mathrm{g}}}{\mathrm{d}\xi}=f_{\mathrm{g}}^{\mathrm{l}}-vS_{\mathrm{g}}-\big(f_{\mathrm{g}}^--vS_{\mathrm{g}}^-\big),\\ S_{\mathrm{w}}(-\infty)=S_{\mathrm{w}}^-,\qquad S_{\mathrm{w}}(0)=S_{\mathrm{w}}^{\mathrm{l}},\\ S_{\mathrm{g}}(-\infty)=S_{\mathrm{g}}^-,\qquad S_{\mathrm{g}}(0)=S_{\mathrm{g}}^{\mathrm{l}} \end{cases} \tag{3.48}$$

and for $\xi > 0$

$$(P^{\mathrm{r}}) \quad \begin{cases} \dfrac{\mathrm{d}S_{\mathrm{w}}}{\mathrm{d}\xi} = u^+ f_{\mathrm{w}}^{\mathrm{r}} - vS_{\mathrm{w}} - \left(u^+ f_{\mathrm{w}}^+ - vS_{\mathrm{w}}^+\right), \\ \dfrac{\mathrm{d}S_{\mathrm{g}}}{\mathrm{d}\xi} = u^+ f_{\mathrm{g}}^{\mathrm{r}} - vS_{\mathrm{g}}, \\ S_{\mathrm{w}}(+\infty) = S_{\mathrm{w}}^+, \qquad S_{\mathrm{w}}(0) = S_{\mathrm{w}}^{\mathrm{r}}, \\ S_{\mathrm{g}}(+\infty) = 0, \qquad S_{\mathrm{g}}(0) = S_{\mathrm{g}}^{\mathrm{r}}, \end{cases} \tag{3.49}$$

where we have used $u^+ f_{\mathrm{g}}^+ - vS_{\mathrm{g}}^+ = 0$. We need to find such boundary values $S_{\mathrm{w}}^-$, $S_{\mathrm{g}}^-$ and $S_{\mathrm{w}}^+$, so that the sub-problems $(P^{\mathrm{l}})$ and $(P^{\mathrm{r}})$ admit a solution with $S_{\mathrm{w}}^{\mathrm{l}} = S_{\mathrm{w}}^{\mathrm{r}}$ and $S_{\mathrm{g}}^{\mathrm{l}} = S_{\mathrm{g}}^{\mathrm{r}}$. For that choice we have continuous transition saturations that satisfy equations (3.43) and (3.44). Only if we make the additional assumption (2.9) about the value of the steam saturation at the SCF, we find unique values $S_{\mathrm{w}}^-$, $S_{\mathrm{g}}^-$ and $S_{\mathrm{w}}^+$. This will be explained in the next section.

### *3.3. Matching conditions*

We first consider problem $(P^{\mathrm{l}})$. To determine the nature of the equilibrium point $(S_{\mathrm{w}}^-, S_{\mathrm{g}}^-)$ we compute the eigenvalues $e_k$ $(k = 1, 2)$ of the linearized system at that point. This yields

$$e_k = \lambda_k - v, \tag{3.50}$$

where $\lambda_k$ are the eigenvalues of the Jacobian matrix $D\mathbf{f}$, see (3.17). Consequently, if we take $(S_{\mathrm{w}}^-, S_{\mathrm{g}}^-) \in \mathcal{D}_l$, we find that $e_1 < e_2 < 0$. This means that no non-trivial orbit is possible that ends up in $(S_{\mathrm{w}}^-, S_{\mathrm{g}}^-)$ as $\xi \to -\infty$. Combining this information with (3.24) we find as remaining possibility $(S_{\mathrm{w}}^-, S_{\mathrm{g}}^-) \in l$: in other words, the saturations at the upstream side of the SCF must satisfy the condition

$$\lambda_2(S_{\mathrm{w}}^-, S_{\mathrm{g}}^-) = v, \tag{3.51}$$

implying that $(S_{\mathrm{w}}^-, S_{\mathrm{g}}^-)$ is a non-hyperbolic saddle for problem 3.48 with $e_1 < e_2 = 0$. Given a pair $(S_{\mathrm{w}}^-, S_{\mathrm{g}}^-)$ satisfying this condition, we find the orbit that represents the solution of problem $(P^{\mathrm{l}})$ by the following shooting procedure. Let $S_{\mathrm{g}}(0)$ be the prescribed value of the steam saturation at the SCF. We fix $S_{\mathrm{g}}^{\mathrm{l}} = S_{\mathrm{g}}(0)$ in problem $(P^{\mathrm{l}})$ and take $S_{\mathrm{w}}^{\mathrm{l}}$ as a shooting parameter: that is, we solve the equations in problem $(P^{\mathrm{l}})$ by a fourth order Runge–Kutta procedure in the negative $\xi$-direction with start values $(S_{\mathrm{w}}^{\mathrm{l}}, S_{\mathrm{g}}^{\mathrm{l}})$. The corresponding orbit will deflect either to the left or to the right, see figure 6(a). Applying the bisection method, one finds after a number of iterations an accurate approximation of the water saturation at the origin $S_{\mathrm{w}}(0) = S_{\mathrm{w}}^{\mathrm{l}}$ for which a solution exists at the given values of $S_{\mathrm{w}}^-, S_{\mathrm{g}}^-$ and $S_{\mathrm{g}}(0)$.

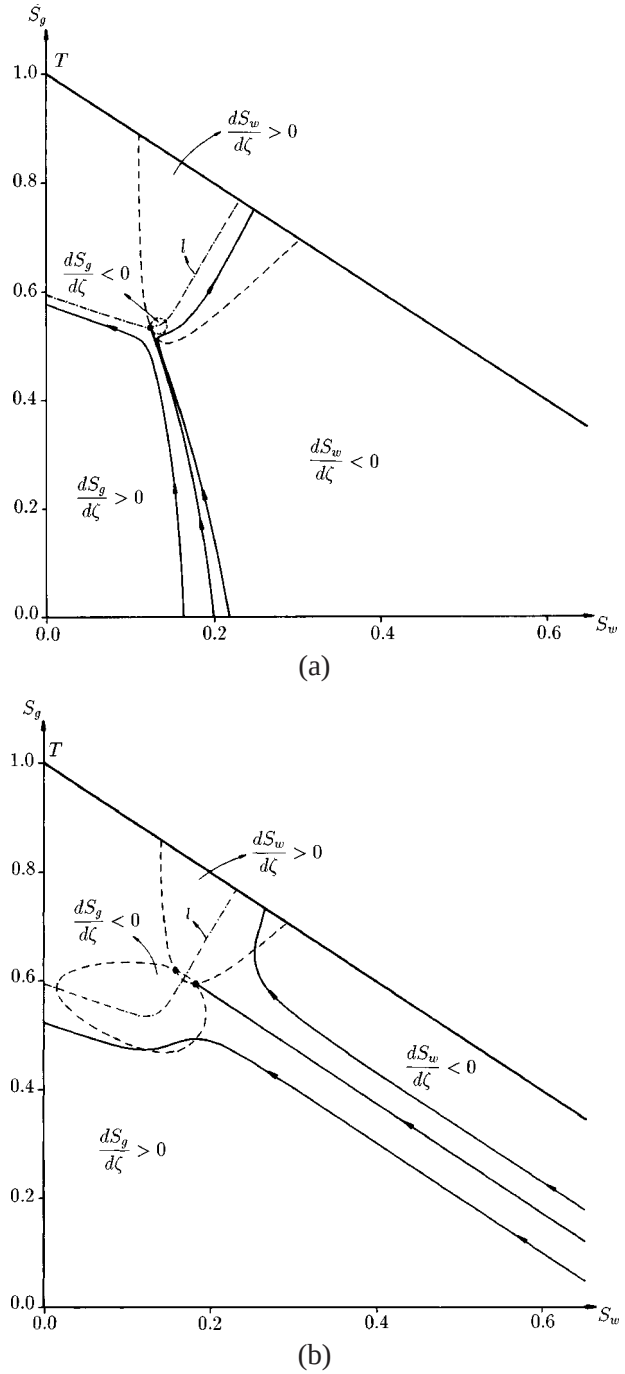


Figure 6. Shooting procedure to solve problem $(P^{\mathrm{l}})$. Here $S_{\mathrm{g}}(0) = 0$. (a) Flow diagram for $(S_{\mathrm{w}}^{-}, S_{\mathrm{g}}^{-}) \in l$. (b) Flow diagram for $(S_{\mathrm{w}}^{-}, S_{\mathrm{g}}^{-}) \in \mathcal{D}_l$. The dots indicate the location of equilibrium points. The orbits are pointing in the negative $\xi$ direction and $\zeta = -\xi$.

At this point it is instructive to consider the dynamics of solutions in the saturation triangle more closely. Because we solve the equations in the negative $\xi$-direction, we put

$$\zeta = -\xi \tag{3.52}$$

and consider the initial value problem

$$\begin{cases} \dfrac{\mathrm{d}S_{\mathrm{w}}}{\mathrm{d}\zeta} = \left(f_{\mathrm{w}}^{-} - vS_{\mathrm{w}}^{-}\right) - f_{\mathrm{w}}^{\mathrm{l}} + vS_{\mathrm{w}}, \\ \dfrac{\mathrm{d}S_{\mathrm{g}}}{\mathrm{d}\zeta} = \left(f_{\mathrm{g}}^{-} - vS_{\mathrm{g}}^{-}\right) - f_{\mathrm{g}}^{\mathrm{l}} + vS_{\mathrm{g}}, \\ S_{\mathrm{w}}(0) = S_{\mathrm{w}}^{\mathrm{l}}, \qquad S_{\mathrm{g}}(0) = S_{\mathrm{g}}^{\mathrm{l}}. \end{cases} \tag{3.53}$$

The qualitative behavior of orbits is determined by the location of equilibrium points and curves where either $\mathrm{d}S_{\mathrm{w}}/\mathrm{d}\zeta = 0$ or $\mathrm{d}S_{\mathrm{g}}/\mathrm{d}\zeta = 0$. This is shown in figure 6 for two locations of $(S_{\mathrm{w}}^{-}, S_{\mathrm{g}}^{-})$. In figure 6(a) we have chosen $(S_{\mathrm{w}}^{-}, S_{\mathrm{g}}^{-}) \in l$. The location of the curves where either $\mathrm{d}S_{\mathrm{w}}/\mathrm{d}\zeta = 0$ or $\mathrm{d}S_{\mathrm{g}}/\mathrm{d}\zeta = 0$ suggests the existence of only one equilibrium point, namely $(S_{\mathrm{w}}^{-}, S_{\mathrm{g}}^{-})$. Three orbits are shown in this figure, all originating from the base line $S_{\mathrm{g}} = 0$: one deflects to the left and one deflects to the right of the equilibrium. The middle orbit approximates the solution that reaches $(S_{\mathrm{w}}^{-}, S_{\mathrm{g}}^{-})$ as $\zeta \to \infty$. In figure 6(b) we have chosen $(S_{\mathrm{w}}^{-}, S_{\mathrm{g}}^{-}) \in \mathcal{D}_l$. The location of the separation curves now suggests the existence of two equilibria: one inside $\mathcal{D}_l$, being the chosen $(S_{\mathrm{w}}^{-}, S_{\mathrm{g}}^{-})$, and one outside $\mathcal{D}_l$. Observe from the sign conditions that no orbit can reach $(S_{\mathrm{w}}^{-}, S_{\mathrm{g}}^{-})$ as $\zeta \to \infty$. This corresponds to the earlier observation about the negative sign of the eigenvalues of the linearized system near that point.

Let us now introduce the additional hypothesis (2.9), expressing that also in the transition zone the steam saturation vanishes at the SCF:

$$S_{\mathrm{g}}(0) = S_{\mathrm{g}}^{\mathrm{l}} = S_{\mathrm{g}}^{\mathrm{r}} = 0. \tag{3.54}$$

Using this assumption we propose the following procedure for problem $(P^{\mathrm{l}})$ . Choose $S_{\mathrm{w}}^{-}$, find the corresponding $S_{\mathrm{g}}^{-}$ so that (3.51) holds and apply the above described shooting procedure with (3.54) to find the water saturation at the SCF. This yields $S_{\mathrm{w}}^{\mathrm{l}}$ as a function of $S_{\mathrm{w}}^{-}$. With values taken from table 1, we computed this function and the result is shown in figure 7. Note that $S_{\mathrm{w}}^{\mathrm{l}}$ depends continuously and monotonically on $S_{\mathrm{w}}^{-}$ and that $S_{\mathrm{w}}^{\mathrm{l}} = 0$ whenever $S_{\mathrm{w}}^{-} = 0$.

Next we consider problem $(P^{\mathrm{r}})$. To prove the existence of a continuous traveling wave we want to express the water saturation just downstream of the SCF in terms of $S_{\mathrm{w}}^{-}$ as well (curve $S_{\mathrm{w}}^{\mathrm{r}}(1)$ in figure 7). To establish this we first need to express $S_{\mathrm{w}}^{+}$ in terms of $S_{\mathrm{w}}^{-}$. This we do by combining $S_{\mathrm{g}}^{+} = 0$, expression (3.51) and the Rankine–Hugoniot condition (3.47). Computations show, see figure 8, that given any $S_{\mathrm{w}}^{-}$ there are two possible values for $S_{\mathrm{w}}^{+}$. However, in view of (3.29), we must restrict ourselves to the lower branch in figure 8, which is a monotonically decreasing

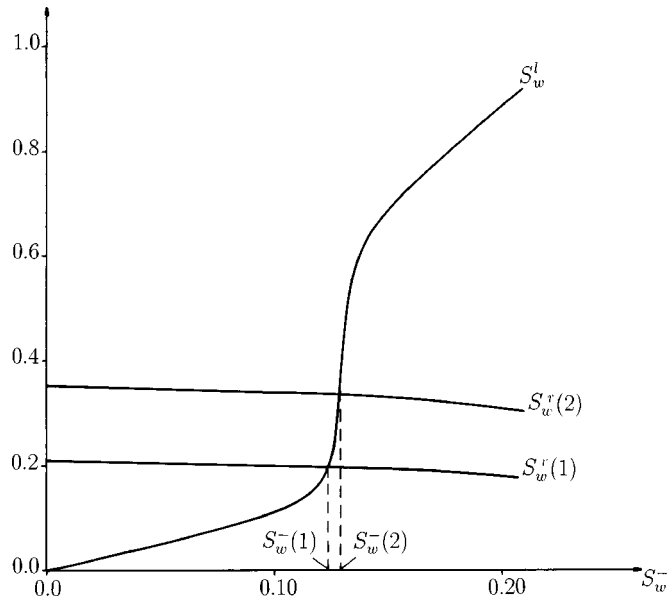


Figure 7. Water saturation at the SCF as a function of $S_w^-$. Curve $S_w^r(1)$ is computed with the base case temperature (2.8) in the transition zone. Curve $S_w^r(2)$ is computed with temperature (2.14) in the transition zone, see section 4.2.

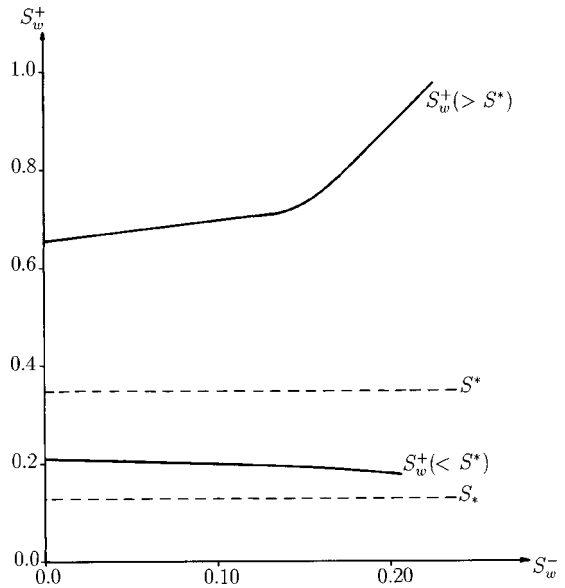


Figure 8. Possible saturation combinations $(S_w^-, S_w^+)$ satisfying the Rankine–Hugoniot conditions (3.47) and condition (3.51).

function of $S_{\mathrm{w}}^{-}$. Note that $S^{*}$ and $S_{*}$ vary slightly with $S_{\mathrm{w}}^{-}$. This dependence enters through $u^{+}$.

How to obtain $S_{\mathrm{w}}^{\mathrm{r}}(1)$ in figure 7? As a result of (3.54) we find $S_{\mathrm{g}}(\xi) = 0$ for all $\xi \geqslant 0$. Therefore, we only need to consider the $S_{\mathrm{w}}$-equation in problem $(P^{\mathrm{r}})$, where we use $T = T_0$ in the coefficients. Writing the water equation as

$$\frac{\mathrm{d}S_{\mathrm{w}}}{\mathrm{d}\xi} = F_{\mathrm{w}}(S_{\mathrm{w}}) = u^{+} f_{\mathrm{w}}^{\mathrm{r}}(S_{\mathrm{w}}) - vS_{\mathrm{w}} - \left\{u^{+} f_{\mathrm{w}}^{\mathrm{r}}\left(S_{\mathrm{w}}^{+}\right) - vS_{\mathrm{w}}^{+}\right\}, \tag{3.55}$$

one easily verifies, as a consequence of (3.29) and (3.31), that $F_{\mathrm{w}}(S_{\mathrm{w}}) > 0$ for $S_{\mathrm{w}} > S_{\mathrm{w}}^{+}$ and $F_{\mathrm{w}}(S_{\mathrm{w}}) < 0$ for $S_{\mathrm{w}} < S_{\mathrm{w}}^{+}$. This implies that the only solution possible is

$$S_{\mathrm{w}}(\xi) = S_{\mathrm{w}}^{+} \quad \text{for all } \xi \geqslant 0. \tag{3.56}$$

Consequently $S_{\mathrm{w}}^{\mathrm{r}} = S_{\mathrm{w}}^{+}$. Therefore, the lower branch in figure 8 also appears as $S_{\mathrm{w}}^{\mathrm{r}}(1)$ in figure 7. By the monotonicity of the curves we find exactly one intersection point at $S_{\mathrm{w}}^{-} = S_{\mathrm{w}}^{-}(1)$. At this point the values of $S_{\mathrm{w}}^{\mathrm{l}}$ and $S_{\mathrm{w}}^{\mathrm{r}}$ are the same, implying continuous water saturation in the transition model. The corresponding values for $S_{\mathrm{g}}^{-}, S_{\mathrm{w}}^{+}$ and $\Lambda$ are found from (3.51), figure 7 and (3.47). The result is:

$$S_{\mathrm{w}}^{-} = S_{\mathrm{w}}^{-}(1) = 0.1240, \qquad S_{\mathrm{g}}^{-} = 0.5339, \qquad S_{\mathrm{w}}^{+} = 0.2014, \qquad \Lambda = 0.9856, \tag{3.57}$$

implying that the steam condensation rate $r$ is approximately equal to the steam injection rate $u_{\mathrm{inj}}$. The $S_{\mathrm{w}}^{+}$-value is such that downstream of the SCF the solution of equation (3.27) consists of a shock only. The composite solution as a path in the saturation–temperature space is shown as curve 1 in figure 9. Note that the transition

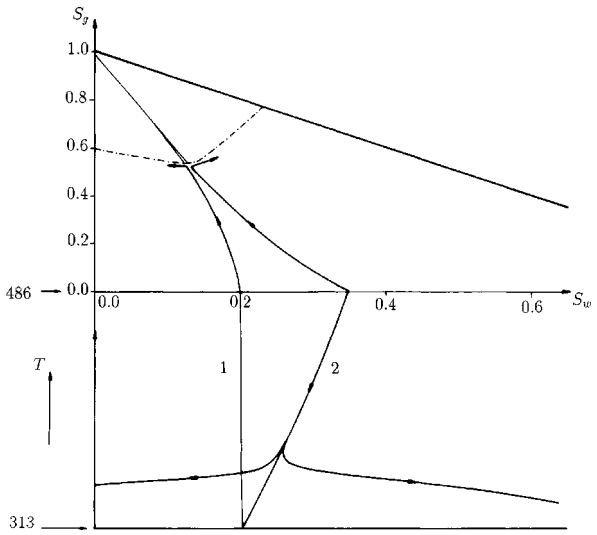


Figure 9. Composite solution as path in the phase–temperature space. Curve 1 reflects the base case, in which the transition temperature is piecewise constant. Curve 2 reflects the continuously varying temperature transition as given by (2.14). Here arrows on the three orbits are pointing in the direction of the shooting procedures.

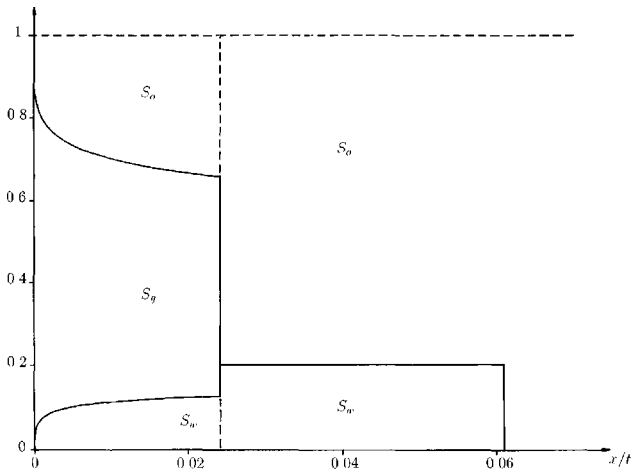


Figure 10. Saturation distribution as a function of $\eta = x/t$.

saturations are monotone functions of $\xi$: $S_{\rm g}$ is decreasing, while $S_{\rm w}$ is increasing. In figure 10 we show the saturations as a function of $\eta = x/t$. This concludes the analysis of the base case.

*Remark.* The solution in the transition region defines a viscous profile for the hyperbolic problem related to the base case. The constructed traveling wave connects the non-hyperbolic saddle at $(S_{\rm w}^-, S_{\rm g}^-)$, located on the curve $l$, and the point $(S_{\rm w}^+, S_{\rm g}^+ = 0)$. This point is a saddle as well, because the eigenvalues satisfy $\lambda_1 = 0$ and $\lambda_2 > v$. Hence $e_1 = -v < 0$ and $e_2 > 0$. Thus the saturation shock at the SCF is a transitional shock in the sense of Isaacson et al. [15].

## 4. Different transition models

In this section we investigate the relation between the transition model and the matching condition at the SCF in the global interface model.

### *4.1. Brooks–Corey capillary pressure diffusion*

To incorporate the capillary pressure expressions (2.10) into the mathematical formulation of the base case, we start from Darcy's law for the individual phases

$$u_i = -k\frac{k_{{\rm r}i}}{\mu_i}\frac{\partial p_i}{\partial x}, \tag{4.1}$$

and use the definitions

$$P_{\rm c}^{\rm ow} = p_{\rm o} - p_{\rm w}; \qquad P_{\rm c}^{\rm go} = p_{\rm g} - p_{\rm o}; \qquad P_{\rm c}^{\rm gw} = p_{\rm g} - p_{\rm w}, \tag{4.2}$$

to eliminate the pressures from the phase velocities. This gives

$$u_{\mathrm{w}} = uf_{\mathrm{w}} + f_{\mathrm{w}}k\frac{k_{\mathrm{ro}}}{\mu_{\mathrm{o}}}\frac{\partial P_{\mathrm{c}}^{\mathrm{ow}}}{\partial x} + f_{\mathrm{w}}k\frac{k_{\mathrm{rg}}}{\mu_{\mathrm{g}}}\frac{\partial P_{\mathrm{c}}^{\mathrm{gw}}}{\partial x}, \tag{4.3}$$

$$u_{\mathrm{o}} = uf_{\mathrm{o}} - f_{\mathrm{o}}k\frac{k_{\mathrm{rw}}}{\mu_{\mathrm{w}}}\frac{\partial P_{\mathrm{c}}^{\mathrm{ow}}}{\partial x} + f_{\mathrm{o}}k\frac{k_{\mathrm{rg}}}{\mu_{\mathrm{g}}}\frac{\partial P_{\mathrm{c}}^{\mathrm{go}}}{\partial x}, \tag{4.4}$$

$$u_{\mathrm{g}} = uf_{\mathrm{g}} - f_{\mathrm{g}}k\frac{k_{\mathrm{ro}}}{\mu_{\mathrm{o}}}\frac{\partial P_{\mathrm{c}}^{\mathrm{go}}}{\partial x} - f_{\mathrm{g}}k\frac{k_{\mathrm{rw}}}{\mu_{\mathrm{w}}}\frac{\partial P_{\mathrm{c}}^{\mathrm{gw}}}{\partial x}, \tag{4.5}$$

where the total discharge $u$ is given by (3.6) and the fractional flow functions $f_i$ by (3.4), with power law relative permeabilities. Substituting these velocities into the phase balance equations and eliminating, as before, the oil saturation yields the modified transition equations for $S_{\mathrm{w}}$ and $S_{\mathrm{g}}$. As in section 3, we recast the equations in dimensionless form to obtain

$$\begin{aligned}&\frac{\partial S_{\mathrm{w}}}{\partial t} + \frac{\partial u f_{\mathrm{w}}}{\partial x}\\ &\quad = \frac{\rho_{\mathrm{g}}}{\rho_{\mathrm{w}}}\Lambda\delta(x-vt) - \varepsilon\frac{\partial}{\partial x}\left\{ f_{\mathrm{w}}(k_{\mathrm{ro}} + k_{\mathrm{rg}}M_{\mathrm{og}})\frac{\partial J^{\mathrm{ow}}}{\partial x} + f_{\mathrm{w}}k_{\mathrm{rg}}M_{\mathrm{og}}\frac{\partial J^{\mathrm{go}}}{\partial x}\right\},\end{aligned} \tag{4.6}$$

$$\begin{aligned}&\frac{\partial S_{\mathrm{g}}}{\partial t} + \frac{\partial u f_{\mathrm{g}}}{\partial x}\\ &\quad = -\Lambda\delta(x-vt) + \varepsilon\frac{\partial}{\partial x}\left\{ f_{\mathrm{g}}(k_{\mathrm{ro}} + k_{\mathrm{rw}}M_{\mathrm{ow}})\frac{\partial J^{\mathrm{go}}}{\partial x} + f_{\mathrm{g}}k_{\mathrm{rw}}M_{\mathrm{ow}}\frac{\partial J^{\mathrm{ow}}}{\partial x}\right\},\end{aligned} \tag{4.7}$$

where we have used $P_{\mathrm{c}}^{\mathrm{gw}} = P_{\mathrm{c}}^{\mathrm{go}} + P_{\mathrm{c}}^{\mathrm{ow}}$ and expressions (2.10) for $P_{\mathrm{c}}^{\mathrm{go}}$ and $P_{\mathrm{c}}^{\mathrm{ow}}$. The Leverett functions follow from (2.10) and (2.12) and the dimensionless number $\varepsilon$ results from (3.34) and (2.13):

$$\varepsilon = \frac{D}{u_{\mathrm{inj}}L} = \frac{\sigma\sqrt{\phi k}}{\mu_{\mathrm{o}}u_{\mathrm{inj}}L}. \tag{4.8}$$

Note that $\varepsilon$ is related to the capillary number (capillary forces/viscous forces). Since we have assumed that $J^{\mathrm{ow}} = J^{\mathrm{ow}}(S_{\mathrm{w}})$ and $J^{\mathrm{og}} = J^{\mathrm{og}}(S_{\mathrm{g}})$, we give equations (4.6) and (4.7) the more convenient form

$$\frac{\partial S_{\mathrm{w}}}{\partial t} + \frac{\partial u f_{\mathrm{w}}}{\partial x} = \frac{\rho_{\mathrm{g}}}{\rho_{\mathrm{w}}}\Lambda\delta(x-vt) + \varepsilon\frac{\partial}{\partial x}\left\{ D_{\mathrm{ww}}\frac{\partial S_{\mathrm{w}}}{\partial x} + D_{\mathrm{wg}}\frac{\partial S_{\mathrm{g}}}{\partial x}\right\}, \tag{4.9}$$

$$\frac{\partial S_{\mathrm{g}}}{\partial t} + \frac{\partial u f_{\mathrm{g}}}{\partial x} = -\Lambda\delta(x-vt) + \varepsilon\frac{\partial}{\partial x}\left\{ D_{\mathrm{gw}}\frac{\partial S_{\mathrm{w}}}{\partial x} + D_{\mathrm{gg}}\frac{\partial S_{\mathrm{g}}}{\partial x}\right\}. \tag{4.10}$$

These equations replace the base case equations (3.35) and (3.36). We now proceed as in section (3.2). That is, we introduce the scaled traveling wave coordinate $\xi$ in equations (4.9) and (4.10) and assume traveling wave type profiles for the solutions. Integrating the resulting ordinary differential equations and applying boundary condi-

tions (3.45), (3.46) yields the same Rankine–Hugoniot conditions as before. Instead of sub-problems $(P^{\mathrm{l}})$ and $(P^{\mathrm{r}})$, we now obtain for $\xi < 0$

$$(Q^{\mathrm{l}}) \quad \begin{cases} D^{\mathrm{l}}_{\mathrm{ww}} \dfrac{\mathrm{d}S_{\mathrm{w}}}{\mathrm{d}\xi} + D^{\mathrm{l}}_{\mathrm{wg}} \dfrac{\mathrm{d}S_{\mathrm{g}}}{\mathrm{d}\xi} = f^{\mathrm{l}}_{\mathrm{w}} - vS_{\mathrm{w}} - \big(f^{-}_{\mathrm{w}} - vS^{-}_{\mathrm{w}}\big), \\ D^{\mathrm{l}}_{\mathrm{gw}} \dfrac{\mathrm{d}S_{\mathrm{w}}}{\mathrm{d}\xi} + D^{\mathrm{l}}_{\mathrm{gg}} \dfrac{\mathrm{d}S_{\mathrm{g}}}{\mathrm{d}\xi} = f^{\mathrm{l}}_{\mathrm{g}} - vS_{\mathrm{g}} - \big(f^{-}_{\mathrm{g}} - vS^{-}_{\mathrm{g}}\big), \\ S_{\mathrm{w}}(-\infty) = S^{-}_{\mathrm{w}}, \qquad S_{\mathrm{w}}(0) = S^{\mathrm{l}}_{\mathrm{w}}, \\ S_{\mathrm{g}}(-\infty) = S^{-}_{\mathrm{g}}, \qquad S_{\mathrm{g}}(0) = 0, \end{cases} \tag{4.11}$$

and for $\xi > 0$

$$(Q^{\mathrm{r}}) \quad \begin{cases} D^{\mathrm{r}}_{\mathrm{ww}} \dfrac{\mathrm{d}S_{\mathrm{w}}}{\mathrm{d}\xi} + D^{\mathrm{r}}_{\mathrm{wg}} \dfrac{\mathrm{d}S_{\mathrm{g}}}{\mathrm{d}\xi} = u^{+} f^{\mathrm{r}}_{\mathrm{w}} - vS_{\mathrm{w}} - \big(u^{+} f^{+}_{\mathrm{w}} - vS^{+}_{\mathrm{w}}\big), \\ D^{\mathrm{r}}_{\mathrm{gw}} \dfrac{\mathrm{d}S_{\mathrm{w}}}{\mathrm{d}\xi} + D^{\mathrm{r}}_{\mathrm{gg}} \dfrac{\mathrm{d}S_{\mathrm{g}}}{\mathrm{d}\xi} = u^{+} f^{\mathrm{r}}_{\mathrm{g}} - vS_{\mathrm{g}}, \\ S_{\mathrm{w}}(+\infty) = S^{+}_{\mathrm{w}}, \qquad S_{\mathrm{w}}(0) = S^{\mathrm{r}}_{\mathrm{w}}, \\ S_{\mathrm{g}}(+\infty) = 0, \qquad S_{\mathrm{g}}(0) = 0, \end{cases} \tag{4.12}$$

where we have used condition (3.54). The upper indices in the diffusion coefficients relate to the temperature difference across the SCF. The properties of the nonlinear functions imply (for $j = \mathrm{l}, \mathrm{r}$)

$$D^{j}_{\mathrm{ww}}, D^{j}_{\mathrm{gg}} > 0 \quad \text{and} \quad D^{j}_{\mathrm{wg}}, D^{j}_{\mathrm{gw}} < 0 \tag{4.13}$$

and

$$D^{j}_{\mathrm{ww}} D^{j}_{\mathrm{gg}} > D^{j}_{\mathrm{wg}} D^{j}_{\mathrm{gw}} \tag{4.14}$$

in $\mathcal{D}$. Because we are modifying only the transition model, conditions (3.24) and (3.29) remain unchanged.

We first consider the solvability of problem $(Q^{\mathrm{l}})$. As in the base case, the behavior of solutions depends critically on the location of the equilibrium point $(S^{-}_{\mathrm{w}}, S^{-}_{\mathrm{g}})$. Inequalities (4.13) and (4.14) imply that the diffusion matrix is positive definite. This means that the number and location of equilibrium points in problems $(Q^{\mathrm{l}})$ and $(P^{\mathrm{l}})$ are identical. Of course, the curves where $\mathrm{d}S_{\mathrm{w}}/\mathrm{d}\xi = 0$ and $\mathrm{d}S_{\mathrm{g}}/\mathrm{d}\xi = 0$ are different. Two typical cases are shown in figure 11, where we again introduced the variable $\zeta = -\xi$ (i.e., we computed orbits in the positive $\zeta$ direction).

As in the base case, equilibrium points $(S^{-}_{\mathrm{w}}, S^{-}_{\mathrm{g}}) \in \mathcal{D}_l$ (figure 11(b)) cannot be reached. What remains is again the possibility $(S^{-}_{\mathrm{w}}, S^{-}_{\mathrm{g}}) \in l$. Selecting points on the curve $l$, corresponding initial points $S^{\mathrm{l}}_{\mathrm{w}}$ were found numerically, yielding a dependence which closely resembles the one shown in figure 7. Observe from figure 11 that now the water saturation in the transition region is not monotone: in the direction of negative $\xi$ it first increases, reaches a global maximum and then decreases towards $S^{-}_{\mathrm{w}}$ at $\xi = -\infty$.

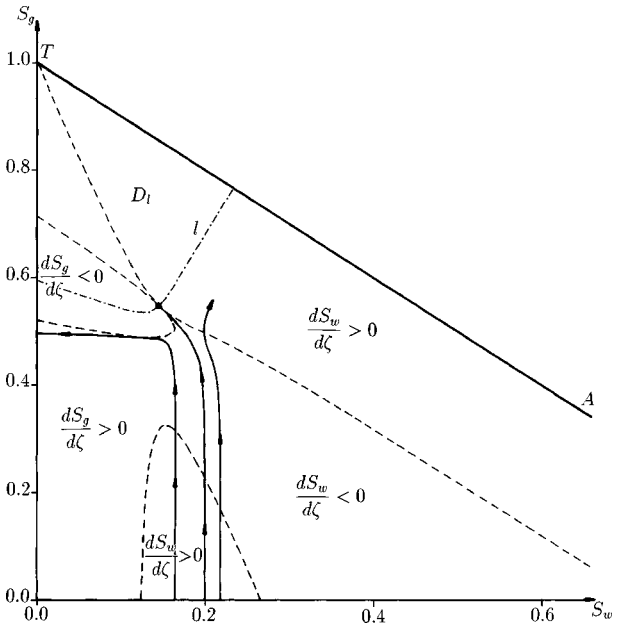


(a)

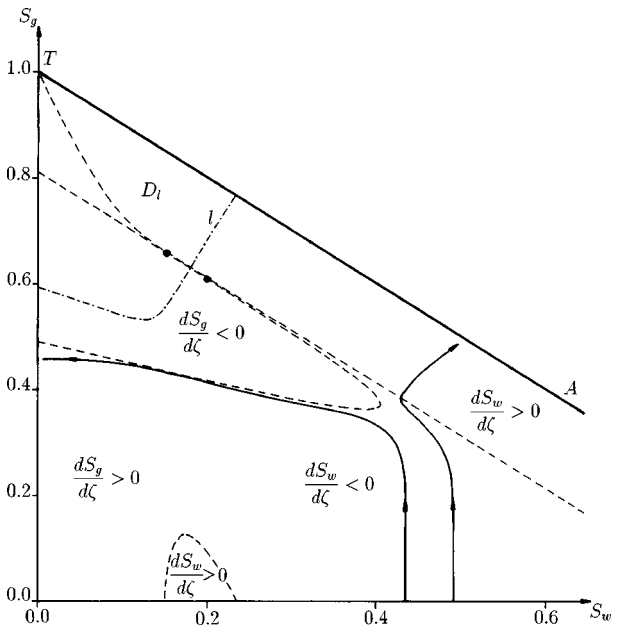


(b)

Figure 11. Shooting procedure to solve problem $(Q^{\mathrm{l}})$. Here $S_{\mathrm{g}}(0) = 0$. (a) Flow diagram for $(S_{\mathrm{w}}^{-}, S_{\mathrm{g}}^{-}) \in l$. (b) Flow diagram for $(S_{\mathrm{w}}^{-}, S_{\mathrm{g}}^{-}) \in \mathcal{D}_l$. The dots indicate the location of equilibrium points. Again $\zeta = -\xi$.

We established computationally that solutions of problem $(Q^{\mathrm{r}})$ satisfy $\mathrm{d}S_{\mathrm{g}}/\mathrm{d}\zeta > 0$ for $S_{\mathrm{g}}$ close to zero. Together with the boundary conditions this implies $S_{\mathrm{g}}(\xi) = 0$ for all $\xi \geqslant 0$. A similar argument as in section 3.3 here again gives $S_{\mathrm{w}}(\xi) = S_{\mathrm{w}}^{+}$ for all $\xi \geqslant 0$. We then apply the procedure outlined in section 3.2 and find for different values of the sorting factor $\lambda_{\mathrm{s}}$, as appearing in expressions (2.12), different interface saturations. Corresponding to $\lambda_{\mathrm{s}} = 2$ there results:

$$S_{\mathrm{w}}^{-} = 0.1452, \qquad S_{\mathrm{g}}^{-} = 0.5467, \qquad S_{\mathrm{w}}^{+} = 0.1990, \qquad \Lambda = 0.9855. \quad (4.15)$$

### *4.2. Temperature variation*

Next we modify the temperature distribution in the transition model. Instead of the discontinuous temperature (2.8), we will now investigate the consequence of the continuous expression (2.14). Clearly this modification leaves the transition model for $\xi < 0$ unchanged. In particular, conditions (3.51) and (3.29), the Rankine–Hugoniot conditions (3.47) and the results for problem $(P^{\mathrm{l}})$, with $S_{\mathrm{g}}(0) = 0$, are the same as in the base case. Thus with reference to figure 7, we use the same $S_{\mathrm{w}}^{l}$ curve.

The only change occurs in problem $(P^{\mathrm{r}})$ where now the temperature variation with $\xi$ enters in the fractional flow functions $(f_i^{\mathrm{r}} = f_i(S_{\mathrm{w}}, S_{\mathrm{g}}, T(\xi))$ through the mobility ratios. This dependence has no consequence for the steam saturation downstream of the SCF. Since $u^{+} f_{\mathrm{g}}^{\mathrm{r}} - v S_{\mathrm{g}} < 0$ for small positive values of $S_{\mathrm{g}}$, the only possible solution satisfying the $S_{\mathrm{g}}$-equation and boundary conditions is $S_{\mathrm{g}}(\xi) = 0$ for all $\xi \geqslant 0$. What remains is the $S_{\mathrm{w}}$-equation

$$\frac{\mathrm{d}S_{\mathrm{w}}}{\mathrm{d}\xi} = u^{+} f_{\mathrm{w}}\big(S_{\mathrm{w}}, T(\xi)\big) - v S_{\mathrm{w}} - \big(u^{+} f_{\mathrm{w}}^{+} - v S_{\mathrm{w}}^{+}\big) \quad (4.16)$$

for $\xi > 0$. Using the exponential relation in (2.14), we write this equation with the temperature as independent variable

$$\frac{\mathrm{d}S_{\mathrm{w}}}{\mathrm{d}T} = \frac{u^{+} f_{\mathrm{w}}(S_{\mathrm{w}}, T) - v S_{\mathrm{w}} - (u^{+} f_{\mathrm{w}}^{+} - v S_{\mathrm{w}}^{+})}{-\alpha(T - T_0)} \quad (4.17)$$

with $T_0 < T < T_1$. The corresponding boundary conditions are

$$S_{\mathrm{w}}(T_0) = S_{\mathrm{w}}^{+} \quad \text{and} \quad S_{\mathrm{w}}(T_1) = S_{\mathrm{w}}^{\mathrm{r}}. \quad (4.18)$$

Because $(T_0, S_{\mathrm{w}}^{+})$ is a singular point of equation (4.17), we solve it backwards in $T$. Thus given a value for $S_{\mathrm{w}}^{+}$, we start at $T = T_1$ and use the iterative shooting method again to obtain an accurate approximation to the corresponding values for $S_{\mathrm{w}}^{\mathrm{r}}$.

In particular, we find for any given $S_{\mathrm{w}}^{-}$ which yields a unique $S_{\mathrm{w}}^{+}$ from figure 8, a unique water saturation at the right hand side of the SCF. This saturation, which is denoted by $S_{\mathrm{w}}^{\mathrm{r}}(2)$ in figure 7, also depends monotonically on $S_{\mathrm{w}}^{-}$. Consequently, there is again exactly one intersection point at $S_{\mathrm{w}}^{-} = S_{\mathrm{w}}^{-}(2)$. As before, the values for $S_{\mathrm{g}}^{-}, S_{\mathrm{w}}^{+}$ and $\Lambda$ are found from (3.51), figure 7 and (3.47):

$$S_{\mathrm{w}}^{-} = S_{\mathrm{w}}^{-}(2) = 0.1288, \qquad S_{\mathrm{g}}^{-} = 0.5337, \qquad S_{\mathrm{w}}^{+} = 0.2010, \qquad \Lambda = 0.9856. \quad (4.19)$$

The composite solution as a path in the saturation–temperature space is shown as curve 2 in figure 9. Note the significant change in the transition region, in particular, the striking non-monotonicity of $S_{\mathrm{w}}$, but the minor change in the hyperbolic part of the path, i.e., the outer solution.

### 4.3. Positive steam saturation at the SCF

Finally, we modify the base case by replacing condition (3.54). Now we assign a positive value $S_{\mathrm{g}}(0)$ to the steam saturation at the SCF. This does not involve conditions (3.51), (3.29) and (3.47), which therefore remain unchanged here. To find the saturations in the transition region, we now have to solve sub-problems $(P^{\mathrm{l}})$ and $(P^{\mathrm{r}})$ subject to $S_{\mathrm{g}}^{\mathrm{l}} = S_{\mathrm{r}}^{\mathrm{r}} = S_{\mathrm{g}}(0) > 0$. With reference to figure 12, we apply iterative shooting procedures starting from the line $S_{\mathrm{g}} = S_{\mathrm{g}}(0)$: problem $(P^{\mathrm{l}})$ is solved backwards in $\xi$ (or, as before, in the positive $\zeta = -\xi$ direction) and problem $(P^{\mathrm{r}})$ is solved forwards in $\xi$.

Given $S_{\mathrm{w}}^{-}$, we first determine $S_{\mathrm{w}}^{+}$ from figure 8 and then solve problems $(P^{\mathrm{l}})$ and $(P^{\mathrm{r}})$ repeatedly to obtain accurate approximations for $S_{\mathrm{w}}^{\mathrm{l}}$ and $S_{\mathrm{w}}^{\mathrm{r}}$. Again this leads

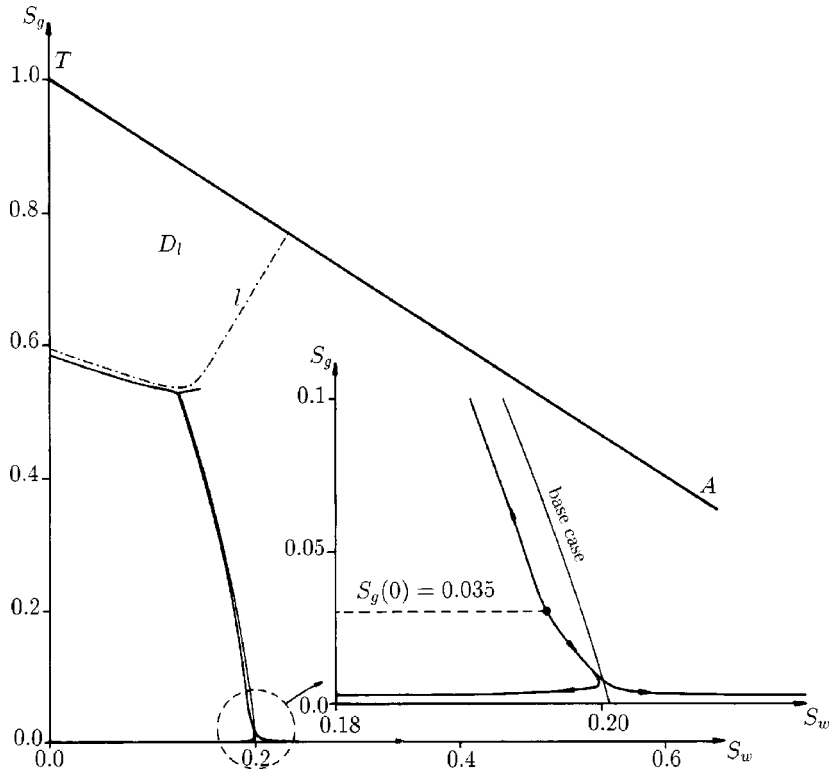


Figure 12. Orbits in the saturation space, starting with a positive value of the steam saturation at the SCF, $S_{\mathrm{g}}(0) > 0$.

to two monotone curves: $S_{\rm w}^{\rm l}$ is increasing and $S_{\rm w}^{\rm r}$ is decreasing with respect to $S_{\rm w}^-$. The unique intersection point gives the required value for $S_{\rm w}^-$. The saturations $S_{\rm g}^-$ and $S_{\rm w}^+$, and the condensation rate $\Lambda$ follow as before. Corresponding to $S_{\rm g}(0) = 0.035$, the result is:

$$S_{\rm w}^- = 0.1237, \qquad S_{\rm g}^- = 0.5339, \qquad S_{\rm w}^+ = 0.2015, \qquad \Lambda = 0.9856. \quad (4.20)$$

Given the parameter values in table 2, one cannot obtain a solution for significant larger $S_{\rm g}(0)$ values. This follows from the sign of the right hand side of the gas equation in problem $(P^{\rm r})$. Taking $S_{\rm w} = 0.2$ in $u^+ f_{\rm g}^{\rm r} - v S_{\rm g}$, one finds that this expression is negative for $0 < S_{\rm g} < 0.04$ and positive for larger $S_{\rm g}$ values. Hence, only when $S_{\rm g}(0)$ is taken in this range a decreasing gas saturation can be constructed. This limitation is a direct consequence of the large viscosity ratio $M_{\rm og}$.

## 5. Parameter variation

Besides the mathematical context, the solutions constructed in sections 3 and 4 are of interest to petroleum engineers, because they can be used to

(1) interpret one-dimensional tube experiments,

(2) validate thermal simulators for steamdrive,

(3) quantify the influence of reservoir and rock properties.

In this section we focus on the parameter dependence, which we investigate for the average oil saturation in the steam zone $\overline{S}_{\rm o}$. Integrating the mass balance for oil, this quantity can be expressed directly in terms of the upstream saturations at the SCF. These saturations result directly from our analysis. As in Dake [3] and Dullien [5] we find

$$\bar{S}_{\rm o} = S_{\rm o}^- - \frac{u}{v} f_{\rm o}\big(S_{\rm w}^-, S_{\rm g}^-\big). \quad (5.1)$$

Now, given a set of model parameters, we compute $S_{\rm w}^-$, $S_{\rm g}^-$ and $S_{\rm o}^-$ as explained in this paper. This analysis, however, is rather involved and it would be desirable to find the upstream saturations by means of a relatively straightforward approximation. With reference to figures 6, 9, 11 and 12 it seems natural to choose the minimum of the curve $l$ for that purpose. Denoting this point by $(S_{\rm w}^{\rm min}, S_{\rm g}^{\rm min}, S_{\rm o}^{\rm min})$ we then have that $S_{\rm w}^{\rm min}$ and $S_{\rm g}^{\rm min}$ satisfy (3.51) for the smallest possible gas saturation. Using these values in (5.1) yields $\overline{S}_{\rm o}^{\rm min}$ as the approximate average oil saturation in the steam zone.

In the parameter variation we change each time only one parameter in table 1. Instead of table 2, we will here use three phase permeabilities. These are obtained by combining Corey two phase relative permeabilities and the modi-

fied Stone I method, see Fayers and Matthews [8]. In full-dimensional form they read:

$$k_{\mathrm{rw}} = k_{\mathrm{rw}}(S_{\mathrm{w}}) = k'_{\mathrm{rw}} S_{\mathrm{we}}^{(2+3\lambda_{\mathrm{s}})/\lambda_{\mathrm{s}}},$$
$$k_{\mathrm{rg}} = k_{\mathrm{rg}}(S_{\mathrm{g}}) = k'_{\mathrm{rg}} S_{\mathrm{ge}}^{2}\big(1 - (1 - S_{\mathrm{ge}})^{(2+\lambda_{\mathrm{s}})/\lambda_{\mathrm{s}}}\big),$$
$$k_{\mathrm{ro}} = k_{\mathrm{ro}}(S_{\mathrm{w}}, S_{\mathrm{g}}) = \frac{S_{\mathrm{o}}}{k_{\mathrm{rcow}}(1 - S_{\mathrm{w}})(1 - S_{\mathrm{ge}})} k_{\mathrm{row}} k_{\mathrm{rog}}.$$

Here,

$$S_{\mathrm{we}} = \frac{S_{\mathrm{w}} - S_{\mathrm{wc}}}{1 - S_{\mathrm{wc}}}, \qquad S_{\mathrm{ge}} = \frac{S_{\mathrm{g}}}{1 - S_{\mathrm{wc}}}$$

and

$$k_{\mathrm{row}} = k'_{\mathrm{rg}}\big(1 - S_{\mathrm{we}}\big)^{2}\big(1 - S_{\mathrm{we}}^{(2+\lambda_{\mathrm{s}})/\lambda_{\mathrm{s}}}\big), \qquad k_{\mathrm{rog}} = k'_{\mathrm{rw}}(1 - S_{\mathrm{ge}})^{(2+3\lambda_{\mathrm{s}})/\lambda_{\mathrm{s}}}.$$

We use $k'_{\mathrm{rw}} = 0.5$ for the end-point permeability of the wetting phase at residual non-wetting phase saturation and $k'_{\mathrm{rg}} = 1.0$ for the end-point permeability of the non-wetting phase at connate wetting phase saturation. Finally, we set $k_{\mathrm{rcow}} = 1$. To describe the effect of oil film flow (oil may spread on water in the presence of steam), the expressions for $k_{\mathrm{row}}$ and $k_{\mathrm{rog}}$ are different from the ones proposed by Fayers and Matthews [8].

Obviously these permeabilities change the nature of the Jacobian matrix (3.16), and in particular of its eigenvalues. They may become complex, yielding an elliptic region in the saturation triangle, see Guzmán and Fayers [12]. However, for our parameter choice ($M_{\mathrm{og}}$ large) the small elliptic region is situated near the $S_{\mathrm{g}} = 0$ axis and plays no role in the analysis.

We show the computational results in figure 13. The vertical axis gives $\overline{S}_{\mathrm{o}}$, as established with the procedure outlined in sections 3 and 4. The horizontal axis shows the "minimum" approximation $\overline{S}_{\mathrm{o}}^{\mathrm{min}}$. Line d in figure 13 shows results for various cold oil viscosities in the medium viscosity range, i.e., 0.09–0.36 [Pa s], using a saturation independent capillary diffusion. Observe that the result is nearly parallel and fairly close to the $\overline{S}_{\mathrm{o}} = \overline{S}_{\mathrm{o}}^{\mathrm{min}}$ line. As to be expected, an increasing oil viscosity leads to a deteriorating displacement efficiency with an increasing oil saturation in the steam zone. In all other cases shown in figure 13, we use Brooks–Corey capillary diffusion. Along line a we again vary the viscosity as for line d. Note the significant differences caused by the different capillary behavior in the transition zone. Along line c we vary the sorting factor $\lambda_{\mathrm{s}}$. This affects both the relative permeabilities and the capillary diffusion. Observe that the deviation from the $\overline{S}_{\mathrm{o}} = \overline{S}_{\mathrm{o}}^{\mathrm{min}}$ line decreases with $\lambda_{\mathrm{s}}$. For reasons of practical interest we also show the effect of different pressures. The steam pressure is not explicit in our equations but affects a number of parameters in table 1. We use empirical relations given by Tortike and Farouq Ali [30] to represent the steam tables. The pressure clearly determines the (boiling) temperature. It also has a small effect on the enthalpy for the conversion of cold water to hot steam ($\Delta H$). Therefore, the steam condensation front velocity decreases at higher pressures,

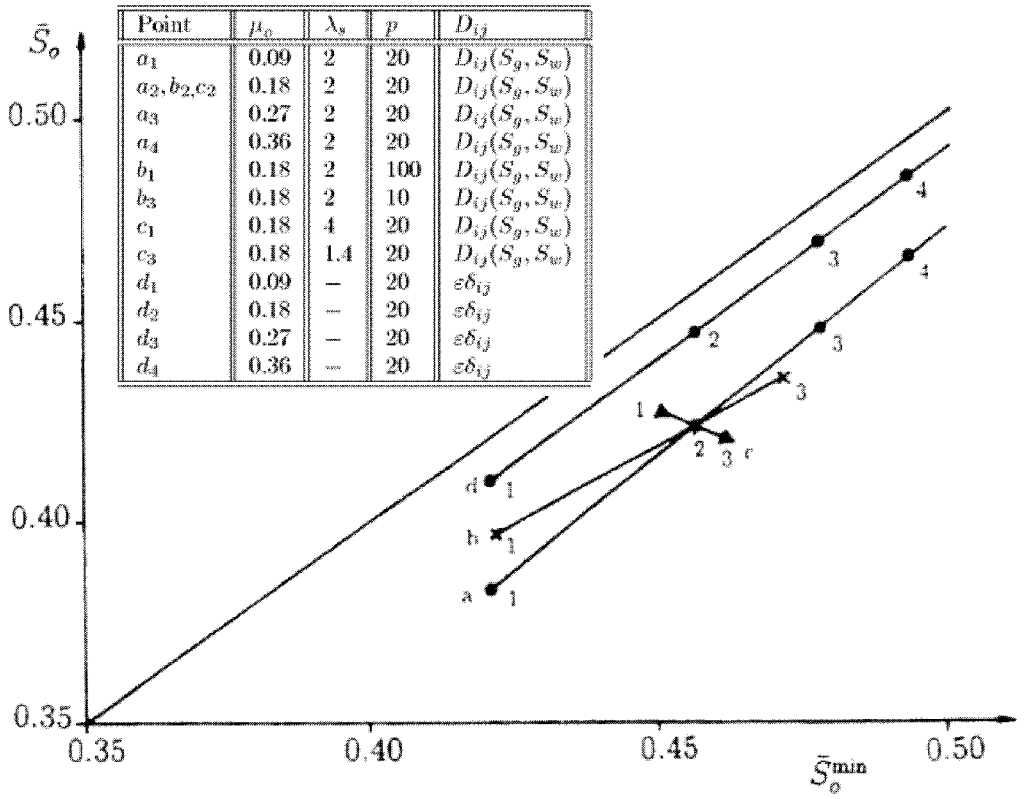


| Point | $\mu_o$ | $\lambda_s$ | $p$ | $D_{ij}$ |
|---|---|---|---|---|
| $a_1$ | 0.09 | 2 | 20 | $D_{ij}(S_g, S_w)$ |
| $a_2, b_2, c_2$ | 0.18 | 2 | 20 | $D_{ij}(S_g, S_w)$ |
| $a_3$ | 0.27 | 2 | 20 | $D_{ij}(S_g, S_w)$ |
| $a_4$ | 0.36 | 2 | 20 | $D_{ij}(S_g, S_w)$ |
| $b_1$ | 0.18 | 2 | 100 | $D_{ij}(S_g, S_w)$ |
| $b_3$ | 0.18 | 2 | 10 | $D_{ij}(S_g, S_w)$ |
| $c_1$ | 0.18 | 4 | 20 | $D_{ij}(S_g, S_w)$ |
| $c_3$ | 0.18 | 1.4 | 20 | $D_{ij}(S_g, S_w)$ |
| $d_1$ | 0.09 | – | 20 | $\varepsilon\delta_{ij}$ |
| $d_2$ | 0.18 | – | 20 | $\varepsilon\delta_{ij}$ |
| $d_3$ | 0.27 | – | 20 | $\varepsilon\delta_{ij}$ |
| $d_4$ | 0.36 | – | 20 | $\varepsilon\delta_{ij}$ |

Figure 13. Comparison of average oil saturation calculated from full computations and calculated with the "approximate minimum condition".

see (2.4). Through its influence on temperature, a high pressure enhances the steam viscosity and lowers the liquid viscosities. Direct pressure effects on viscosities are negligible. The pressure range is between 10 and 100 bar. Indeed the displacement efficiency improves with increasing pressure. Note that this occurs at the expense of a much higher mass of injected steam per unit volume of recovered oil, because higher temperatures are involved now; the reservoir must be heated to a higher temperature.

## 6. Conclusions

Based on the results of this paper we conclude the following:

- The steamdrive model considered in this paper gives a transitional shock wave at the steam condensation front.
- As a consequence, the shock conditions at the steam condensation front inherit details of the local parabolic transition model.
- The presence of steam in the downstream part of the transition zone has no significant effect on the results.

- The rate of temperature decline has no significant effect outside the transition zone, i.e., in the hyperbolic limit.
- The effect of Brooks–Corey capillary diffusion instead of constant (saturation independent) capillary diffusion is well noticeable and cannot be disregarded.
- An approximate solution is given, based on the minimum of the $l$-curve in domain $\mathcal{D}$. The validity of this approximation can be checked from figure 13 for different values of the model parameters.
- The water saturation is significantly non-monotone when considering a continuous temperature decline in the transition region (figure 9). The maximum does not depend on the small parameter $\varepsilon$ and persists in the hyperbolic limit.

## Acknowledgements

The authors wish to thank the anonymous referees for their positive criticism and valuable remarks. Their comments greatly improved this paper. This paper was revised while the authors enjoyed the hospitality of the Institute for Mathematics and its Applications (IMA) in Minnesota.

## References

[1] K. Aziz and A. Settari, *Petroleum Reservoir Simulation* (Applied Science, London, 1979).
[2] J. Bruining, D.W. Batenburg, H.J. van De Haan, R. Quak and C.T.S. Palmgren, The efficiency of the distillation mechanisms to enhance steamdrive recovery, in: *Proc. of the 4th Symposium on Enhanced Oil Recovery*, Hamburg (October 1987).
[3] L.P. Dake, *Fundamentals of Reservoir Engineering* (Elsevier Science, Amsterdam, 1978).
[4] W.B. Dantas, M.E. Gomes, D. Marchesin and Da-Mota, Combustion fronts in petroleum reservoirs, Revista Matemática Contemporânea 8 (1995) 129–149.
[5] F.A.L. Dullien, *Porous Media; Fluid Transport and Pore Structure* (Academic Press, New York, 1979).
[6] A.H. Falls and W.M. Schulte, Theory of three-component, three-phase displacement in porous media, SPE Reservoir Engineering (1992) 377–384.
[7] S.M. Farouq Ali, Q. Doan, R.C.M. Matthias and A.E. George, Study of steamflood performance in stratified reservoirs, in: *Proc. of the 45th Annual Technical Meeting of the Petroleum Society of CIM*, Calgary (June 1994).
[8] F.J. Fayers and J.D. Matthews, Evaluation of normalized Stone's methods for estimating three-phase relative permeabilities, Soc. Petroleum Engrg. J. (1984) 224–232.
[9] J. Glimm, The interaction of nonlinear hyperbolic waves, Comm. Pure Appl. Math. 41 (1988) 569–590.
[10] R.R.G.G. Godderij, J. Bruining and J. Molenaar, A fast 3D interface simulator for steam drives, in: *SPE-Western Regional Meeting* (June 1997) pp. 279–289 (SPE-38288); ibid. SPE Journal 4 (1999) 400–408.
[11] F. Gümrah, C.T.S. Palmgren, J. Bruining and R.R.G.G. Godderij, Steamdrive in a layered reservoir: an experimental and theoretical study, in: *Proc. SPE/DOE 8th Symposium on Enhanced Oil Recovery*, Tulsa (April 1992) pp. 159–167 (SPE/DOE 24171).
[12] R.E. Guzmán and F.J. Fayers, Mathematical properties of three-phase flow equations, SPE Journal 2 (1997) 291–300.

[13] R.E. Guzmán and F.J. Fayers, Solutions to the three-phase Buckley–Leverett problem, SPE Journal 2 (1997) 301–311.
[14] F.G. Hellferich, Theory of multi-component, multi-phase displacement in porous media, Soc. Petroleum Engrg. J. 271 (1981) 51–74.
[15] E. Isaacson, D. Marchesin and B. Plohr, Transitional waves for conservation laws, SIAM J. Math. Anal. 21 (1990) 837–866.
[16] E. Isaacson, D. Marchesin, B. Plohr and J.B. Temple, Multi-phase flow models with singular Riemann problems, Math. Appl. Comput. 11(2) (1992) 147–166.
[17] K.D. Kimber, S.M. Farouq Ali and V.R. Puttagunta, New scaling criteria and their relative merits for steam recovery experiments, J. Cdn. Pet. Tech. 27 (1988) 86–94.
[18] P. Lax, The formation and decay of shock waves, Amer. Math. Monthly 79 (1972) 227–241.
[19] R.J. LeVeque, *Numerical Methods for Conservation Laws* (Birkhäuser, Basel, 1992).
[20] G. Mandl and C.W. Volek, Heat and mass transport in steamdrive processes, Soc. Petroleum Engrg. J. (1969) 57–79.
[21] D. Marchesin, D. Schaeffer, M. Shearer and P.G. Paes-Leme, The classification of $2 \times 2$ systems of non-strictly hyperbolic conservation laws, with application to oil recovery, Comm. Pure Appl. Math. 40 (1987) 141–178.
[22] D.K. Menegus and K.S. Udell, A study of steam injection into water saturated porous media, Heat Transfer in Porous Media and Particle Flows, ASME Heat Transfer Div., New York 46 (1985) 151–157.
[23] C.A. Miller, Stability of moving surfaces in fluid systems with heat and mass transport, III. Stability of displacement fronts in porous media, AIChE Journal 21 (1975) 474–479.
[24] G.A. Pope, The application of fractional flow theory to enhanced oil recovery, Soc. Petroleum Engrg. J. 20 (1980) 191–205.
[25] M. Prats, *Thermal Recovery*, SPE Henry L. Doherty Series, Vol. 7 (SPE, Dallas, 1982).
[26] R.C. Reid, J.M. Prausnitz and T.K. Sherwood, *The Properties of Gases and Liquids* (McGraw-Hill, New York, 1977).
[27] N.D. Shutler, A one dimensional analytical technique for predicting oil recovery by steam flooding, Soc. Petroleum Engrg. J. (1972) 489–498.
[28] J. Smoller, *Shock Waves and Reaction–Diffusion Equations* (Springer, New York, 1980).
[29] L.D. Stewart and K.S. Udell, Mechanisms of residual oil displacement by steam injection, SPE Reservoir Engineering (1988) 1233–1242.
[30] W.S. Tortike and S.M. Farouq Ali, Saturated-steam-property functional correlations for fully implicit thermal reservoir simulation, SPE Reservoir Engineering (1989) 471–474.
[31] K.S. Udell, The thermodynamics of evaporation and condensation in porous media, in: *California Regional Meeting of the Society of Petroleum Engineers*, San Francisco (March 1982) (SPE 10779).
[32] J.S. Wingard and F.M. Orr, An analytical solution for steam/oil/water displacements, SPE Advanced Technology Series 2 (1994) 167–176.
[33] Y.C. Yortsos, Distribution of fluid phases within the steam zone in steam injection processes, Soc. Petroleum Engrg. J. (1984) 458–466.